Electronic Supplementary Information

Biomimetic catalytic oxidative coupling of thiols by thiolate-bridged dinuclear metal complexes containing iron in water under mild conditions

Yahui Zhang,[a] Dawei Yang,*[a] Ying Li,[a] Xiangyu Zhao,[a] Baomin Wang[a] and Jingping Qu*[a,b]

[a]State Key Laboratory of Fine Chemicals, Dalian University of Technology, Dalian 116024, P. R. China

[b]Key Laboratory for Advanced Materials, East China University of Science and Technology, Shanghai 200237, P. R. China

*E-mail: qujp@dlut.edu.cn

yangdw@dlut.edu.cn

Table of Contents

I. Experimental Procedures and Analytical Data

General procedures for 2[PF_6]-catalyzed oxidation of thiophenol in organic solvent.

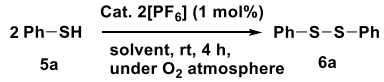

To a Schlenk tube equipped with a magnetic stir bar were added with **2[PF_6]** (13 mg, 0.018 mmol), solvent (2 mL), thiophenol (185 μL, 1.8 mmol), then the resulting solution was stirred in the O_2 atmosphere for 4 h at room temperature. After the reaction solution was concentrated *in vacuum* and extracted with Et_2O (3×10 mL). The combined organic layers were dried with anhydrous Na_2SO_4 and the solvent was removed under reduced pressure. The crude product was purified by flash chromatography using Et_2O.

General procedures for catalytic performance of 2[PF_6], 8[PF_6] and 9[BPh_4] in oxidation of thiophenol in THF-d_8.

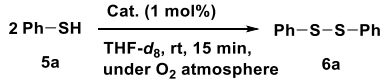

To a Schlenk tube equipped with a magnetic stir bar were added with catalyst (0.018 mmol), THF-d_8 (0.6 mL), thiophenol (185 μL, 1.8 mmol), then the resulting solution was stirred in the O_2 atmosphere for 15 min at room temperature.

General procedures for catalytic performance of some metal complexes in oxidation of thiophenol in aqueous medium.

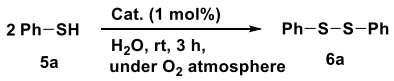

To a Schlenk tube equipped with a magnetic stir bar were added with catalyst (0.018 mmol), H_2O (2 mL), thiophenol (185 μL, 1.8 mmol), then the resulting solution was stirred in the O_2 atmosphere for 3 h at room temperature. After the resulting solution was concentrated *in vacuum* and extracted with Et_2O (3×10 mL). The combined organic layers were dried with anhydrous Na_2SO_4 and the solvent was removed under reduced pressure. The crude product was purified by flash chromatography using Et_2O.

General Procedures for 2[PF_6]-catalyzed oxidation of thiols in aqueous medium.

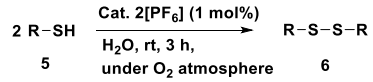

To a Schlenk tube equipped with a magnetic stir bar were added **2[PF_6]** (13 mg, 0.018 mmol), H_2O (2 mL), thiol (1.8 mmol), then the resulting solution was stirred in the O_2 atmosphere for 3 h at room temperature.

Diphenyl disulfide (6a)

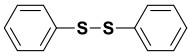

Following the general procedure, the resulting solution was concentrated *in vacuum* and extracted with Et_2O (3×10 mL). Then the combined organic layers were dried with anhydrous Na_2SO_4 and the solvent was removed under reduced pressure. The crude product was purified by flash chromatography using Et_2O. The title compound was obtained as colorless solids in 90% yield. ^{1}H NMR (400 MHz, $CDCl_3$, ppm): δ 7.22-7.25 (m, 2H), 7.29-7.33 (m, 4H), 7.50-7.52 (m, 4H). ^{13}C NMR (100 MHz, $CDCl_3$, ppm): δ 127.29, 127.68, 129.19, 137.18. The ^{1}H and ^{13}C NMR spectral data are in agreement with the literature data.[1,2]

Bis(4-methylphenyl) disulfide (6b)

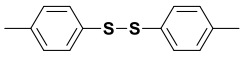

Following the general procedure, the resulting solution was concentrated *in vacuum* and extracted with Et_2O (3×10 mL). Then the combined organic layers were dried with anhydrous Na_2SO_4 and the solvent was removed under reduced pressure. The crude product was purified by flash chromatography using Et_2O. The title compound was obtained as colorless solids in 90% yield. ^{1}H NMR (400 MHz, $CDCl_3$, ppm): δ 2.34 (s, 6H), 7.11 (d, J = 7.8 Hz, 4H), 7.40 (d, J = 8.0 Hz, 4H). ^{13}C NMR (100 MHz, $CDCl_3$, ppm): δ 21.18, 128.69, 129.91, 134.05, 137.56. The ^{1}H and ^{13}C NMR spectral data are in agreement with the literature data.[1,3]

Bis(4-chlorophenyl) disulfide (6c)

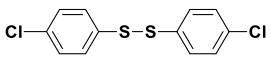

Following the general procedure, the resulting solution was concentrated *in vacuum* and extracted with Et_2O (3×10 mL). Then the combined organic layers were dried with anhydrous Na_2SO_4 and the solvent was removed under reduced pressure. The crude product was purified by flash chromatography using Et_2O. The title compound was obtained as colorless solids in 89% yield. ^{1}H NMR (400 MHz, $CDCl_3$, ppm): δ 7.27 (d, J = 8.6 Hz, 4H), 7.39 (d, J = 8.6 Hz, 4H). ^{13}C NMR (100 MHz, $CDCl_3$, ppm): δ 129.45, 129.47, 133.78, 135.27. The ^{1}H and ^{13}C NMR spectral data are in agreement with the literature data.[1,3]

Bis(phenylmethyl) disulfide (6d)

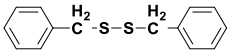

Following the general procedure, the resulting solution was concentrated *in vacuum* and extracted with Et_2O (3×10 mL). Then the combined organic layers were dried with anhydrous Na_2SO_4 and the solvent was removed under reduced pressure. The crude product was purified by flash chromatography using Et_2O. The title compound was obtained as colorless solids in 82% yield. ^{1}H NMR (400 MHz, $CDCl_3$, ppm): δ 3.61 (s, 4H), 7.24-7.34 (m, 10H). ^{13}C NMR (100 MHz, $CDCl_3$, ppm): δ 43.40, 127.53, 128.59, 129.52, 137.48. The ^{1}H and ^{13}C NMR spectral data are in agreement with the literature data.[1,3]

L-Cystine (6e)

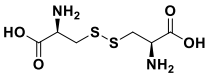

Following the general procedure, the soluion was treated with 5% hydrochloric acid solution since the reaction product was insoluble in water and it was seprarated from the catalyst by filtering. Then, the filtrate was eliminated *in vacuum* to give cystine·HCl as colorless solids. The yield of cystine is 97% based on the amount of cystine·HCl. ^{1}H NMR (400 MHz, 4% NaOD in D_2O, ppm): δ 3.30 (dd, J = 15.2, 7.9 Hz, 2H), 3.44 (dd, J = 15.2, 4.3 Hz, 2H), 4.46 (dd, J = 7.9, 4.3 Hz, 2H). ^{13}C NMR (100 MHz, 4% NaOD in D_2O, ppm): δ 43.56, 54.89, 180.89. The ^{1}H and ^{13}C NMR spectral data are in agreement with the literature data.[1]

Glutathione disulfide (6f)

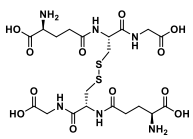

Following the general procedure, after filtration the solvent was removed under reduced pressure and the residue was washed with Et_2O (3×5 mL). The title compound was obtained as colorless solids in 94% yield. ^{1}H NMR (400 MHz, D_2O, ppm): δ 1.19 (t, J = 7.1 Hz, 2H), 2.17 (dd, J = 14.2, 7.4 Hz, 2H), 2.56 (m, 2H), 2.99 (dd, J = 14.3, 9.3 Hz, 2H), 3.29 (dd, J = 14.3, 4.7 Hz, 2H), 3.65 (q, J = 7.1 Hz, 2H), 3.83 (t, J = 6.4 Hz, 2H), 3.98 (s, 4H), 4.75-4.77 (m, 2H). ^{13}C NMR (100 MHz, D_2O, ppm): δ 25.44, 30.94, 38.63, 41.16, 52.25, 52.55, 171.54, 172.56, 172.86, 174.39. The ^{1}H and ^{13}C NMR spectral data are in agreement with the literature data.[1]

II. References

1 M. Oba, K. Tanaka, K. Nishiyama and W. Ando, *J. Org. Chem.*, 2011, **76**, 4173−4177.

2 Y. Li, C. Nie, H. Wang, X. Li, F. Verpoort and C. Duan, *Eur. J. Org. Chem.*, 2011, 7331−7338.

3 T. Tankam, K. Poochampa, T. Vilaivan, M. Sukwattanasinitt and S. Wacharasindhu, *Tetrahedron*, 2016, **72**, 788−793.

III. Catalytic Reaction Screening

Table S1. Solvent screening[a]

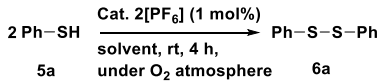

Entry	Solvent	Conversion[b] (%)	Yield[b] (%)
1	Toluene	67	62
2	Et_2O	27	19
3	MeCN	82	67
4	CH_2Cl_2	33	32
5	$^{i}Pr_2O$	45	33
6	THF	100	95

[a]Reaction conditions: thiophenol (1.8 mmol), **2[PF$_6$]** (0.018 mmol), solvent (2 mL), under an O_2 atmosphere, rt, 4 h. [b]Determined by ^{1}H NMR spectroscopy using hexamethylbenzene as an internal standard.

Table S2. Catalyst loading screening[a]

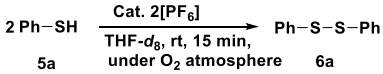

Entry	**2[PF$_6$]** (mol%)	Conversion[b] (%)	Yield[b] (%)
1	1	100	95
2	0.5	87	82
3	0.1	37	33

[a]Reaction conditions: thiophenol (1.8 mmol), **2[PF$_6$]**, THF-d_8 (0.6 mL), under an O_2 atmosphere, rt, 15 min. [b]Determined by ^{1}H NMR spectroscopy using hexamethylbenzene as an internal standard.

Table S3. The change of conversion rate with time[a]

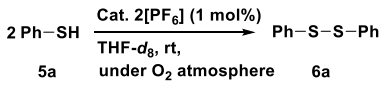

Entry	Time (min)	Conversion[b] (%)	Yield[b] (%)
1	5	84	83
2	10	98	94
3	15	100	95
4	20	100	95

[a]Reaction conditions: thiophenol (1.8 mmol), **2[PF$_6$]** (0.018 mmol), THF-d_8 (0.6 mL), under an O_2 atmosphere, rt. [b]Determined by ^{1}H NMR spectroscopy using hexamethylbenzene as an internal standard.

Figure S1. Time-dependent conversion plot for the aerobic oxidation of thiophenol with **2[PF$_6$]** as the catalyst in THF-d_8

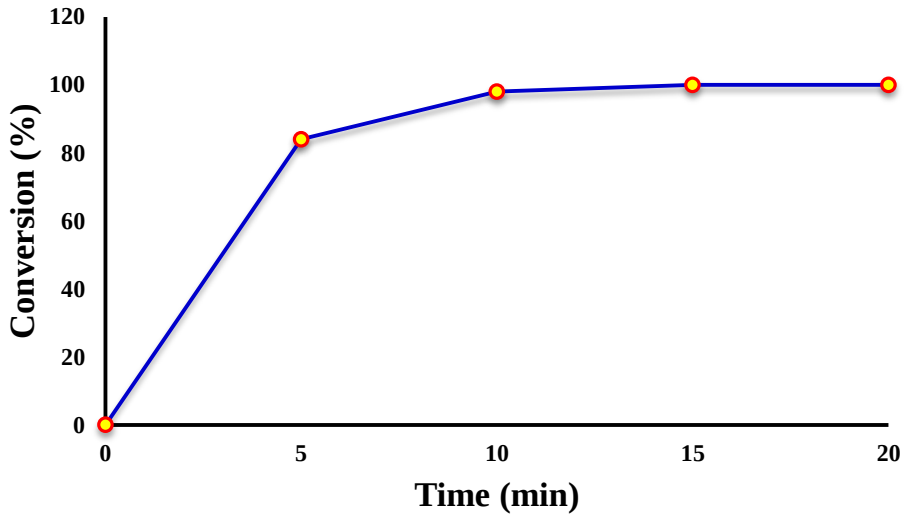

Table S4. Catalytic performance of **2[PF$_6$]**, **8[PF$_6$]** and **9[BPh$_4$]** in oxidation of thiophenol[a]

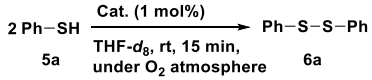

Entry	Catalyst	Conversion[b] (%)	Yield[b] (%)
1	**2[PF$_6$]**	100	95
2	**8[PF$_6$]**	100	96
3	**9[BPh$_4$]**	59	43

[a]Reaction conditions: thiophenol (1.8 mmol), catalyst (0.018 mmol), THF-d_8 (0.6 mL), under an O_2 atmosphere, rt, 15 min. [b]Determined by ^{1}H NMR spectroscopy using hexamethylbenzene as an internal standard.

Table S5. Catalytic performance of some metal complexes in oxidation of thiophenol in aqueous medium[a]

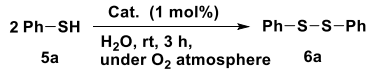

Entry	Catalyst	Conversion[b] (%)	Yield[b] (%)
1	$FeCl_2$	62	3
2	$FeCl_3$	18	9
3	$RuCl_3$	79	12
4	[Cp*Fe(MeCN)$_3$][PF$_6$]	98	70
5	[Cp*Ru(MeCN)$_3$][PF$_6$]	44	14
6	[Cp*Fe(tpdt)FeCp*][PF$_6$]	100	88
7	**2[PF$_6$]**	100	90

[a]Reaction conditions: thiophenol (1.8 mmol), catalyst (0.018 mmol), H_2O (2 mL), under an O_2 atmosphere, rt, 3 h. [b]Determined by ^{1}H NMR spectroscopy using hexamethylbenzene as an internal standard.

IV. EPR Spectrum

Figure S2. The EPR spectrum of **2[PF_6]** at 298K

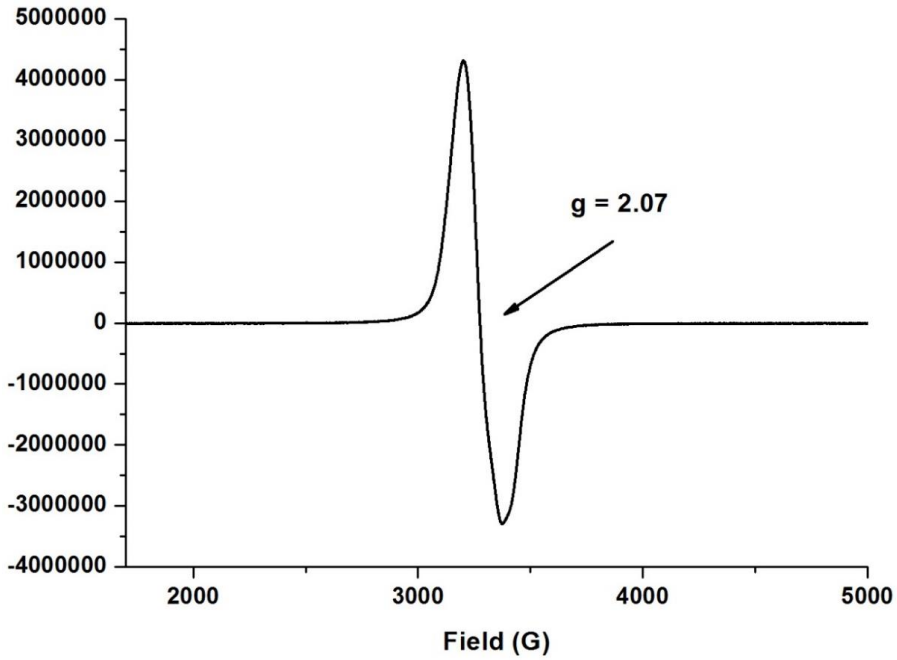

V. X-ray Crystallographic Data

Table S6. Crystal data and structural refinement for complexes **2[PF_6]** and **3**

Complex	**2[PF_6]**	**3**
Formula	$C_{24}H_{38}FeRuS_3PF_6$	$C_{14}H_{23}CoS_3$
Formula weight	724.61	346.43
Crystal dimensions (mm^3)	0.20 × 0.18 × 0.14	0.26 × 0.18 × 0.11
Crystal system	Orthorhombic	Monoclinic
Space group	Cmca	P21/c
a (Å)	15.867(2)	13.1028(9)
b (Å)	20.073(2)	8.6112(6)
c (Å)	18.513(2)	14.2219(10)
α (°)	90.00	90.00
β (°)	90.00	101.5506(13)
γ (°)	90.00	90.00
Volume ($Å^3$)	5896.1(12)	1572.17(19)
Z	8	4
T (K)	296(2)	173(2)
D_{calcd} ($g\ cm^{-3}$)	1.633	1.464
μ (mm^{-1})	1.322	1.471
F (000)	2952	728
No. of rflns. collected	12234	15180
No. of indep. rflns. /R_{int}	2702 / 0.0519	2755 / 0.0553
No. of obsd. rflns. [$I_0 > 2\sigma(I_0)$]	2172	2517
Data / restraints / parameters	2702 / 147 / 190	2755 / 0 / 163
R_1 / wR_2 [$I_0 > 2\sigma(I_0)$]	0.0667 / 0.2143	0.0328 / 0.0884
R_1 / wR_2 (all data)	0.0788 / 0.2248	0.0366 / 0.0913
GOF (on F^2)	1.069	1.062
Largest diff. peak and hole (e $Å^{-3}$)	1.441 / −0.952	0.604 / −0.424
CCDC No.	1837831	1869707

Table S7. Crystal data and structural refinement for complexes **4a[BPh$_4$]** and **4b[BPh$_4$]**

Complex	**4a[BPh$_4$]**	**4b[BPh$_4$]**
Formula	$C_{48}H_{58}BCoFeS_3$	$C_{47}H_{56}BCoFeS_3$
Formula weight	856.71	842.68
Crystal dimensions (mm^3)	0.29 × 0.17 × 0.14	0.29 × 0.21 × 0.15
Crystal system	Orthorhombic	Orthorhombic
Space group	Pna21	Pna21
a (Å)	20.2817(11)	20.576(2)
b (Å)	17.2944(9)	16.9755(19)
c (Å)	12.4241(7)	12.0227(14)
α (°)	90.00	90.00
β (°)	90.00	90.00
γ (°)	90.00	90.00
Volume (Å^3)	4357.9(4)	4199.4(8)
Z	4	4
T (K)	243(2)	200(2)
D_{calcd} (g cm^{-3})	1.306	1.333
μ (mm^{-1})	0.889	0.922
F (000)	1808	1776
No. of rflns. collected	98611	89986
No. of indep. rflns. /R_{int}	7666 / 0.0554	7390 / 0.1014
No. of obsd. rflns. [$I_0 > 2\sigma(I_0)$]	6837	6566
Data / restraints / parameters	7666 / 15 / 487	7390 / 7 / 479
R_1 / wR_2 [$I_0 > 2\sigma(I_0)$]	0.0331 / 0.0817	0.0487 / 0.1108
R_1 / wR_2 (all data)	0.0419 / 0.0862	0.0589 / 0.1155
GOF (on F^2)	1.015	1.099
Largest diff. peak and hole (e Å^{-3})	0.303 / −0.308	0.487 / −0.369
CCDC No.	1869214	1869211

Table S8. Crystal data and structural refinement for complexes **7[PF$_6$]$_2$**, **8[PF$_6$]** and **9[BPh$_4$]**

Complex	**7[PF$_6$]$_2$**	**8[PF$_6$]**	**9[BPh$_4$]**
Formula	$C_{26}H_{41}FeRuS_3NP_2F_{12}$	$C_{30}H_{43}FeRuS_4PF_6$	$C_{48}H_{59}FeRuS_3B$
Formula weight	910.64	833.77	899.86
Crystal dimensions (mm^3)	0.38 × 0.27 × 0.16	0.29 × 0.21 × 0.17	0.25 × 0.21 × 0.19
Crystal system	Orthorhombic	Monoclinic	Monoclinic
Space group	Pnma	P21/n	P21/n
a (Å)	11.800(4)	14.3616(6)	15.5349(4)
b (Å)	15.608(6)	13.9373(6)	15.8332(5)
c (Å)	18.603(7)	16.9737(7)	18.3897(5)
α (°)	90.00	90.00	90.00
β (°)	90.00	99.0564(10)	90.6940(12)
γ (°)	90.00	90.00	90.00
Volume (Å^3)	3426(2)	3355.1(2)	4522.9(2)
Z	4	4	4
T (K)	298(2)	223(2)	173(2)
D_{calcd} (g cm^{-3})	1.765	1.651	1.321
μ (mm^{-1})	1.227	1.234	0.824
F (000)	1840	1704	1880
No. of rflns. collected	72332	42738	40195
No. of indep. rflns. /R_{int}	3133 / 0.0604	5908 / 0.0498	7975 / 0.0474
No. of obsd. rflns. [$I_0 > 2\sigma(I_0)$]	2797	5394	6801
Data / restraints / parameters	3133 / 246 / 235	5908 / 0 / 376	7975 / 1 / 492
R_1 / wR_2 [$I_0 > 2\sigma(I_0)$]	0.0712 / 0.2214	0.0509 / 0.1336	0.0330 / 0.0840
R_1 / wR_2 (all data)	0.0784 / 0.2310	0.0559 / 0.1377	0.0426 / 0.0879
GOF (on F^2)	1.079	1.089	1.078
Largest diff. peak and hole (e Å^{-3})	2.796 / −1.463	3.471 / −3.105	0.522 / −0.649
CCDC No.	1837832	1837835	1843162

Figure S3. ORTEP diagram of **2[PF_6]**

Thermal ellipsoids are shown at 50% probability level. One PF_6 anion and all hydrogen atoms on carbons are omitted for the sake of clarity.

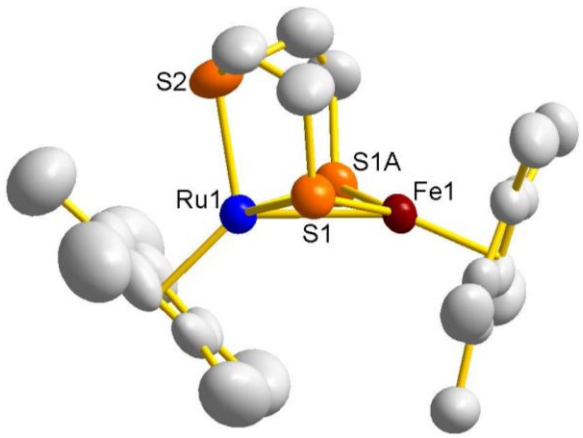

Table S9. Selected bond distances and angles for **2[PF_6]**

Distances (Å)			
Fe1–Ru1	2.691(2)	Ru1–S1	2.305(2)
Fe1–S1	2.197(2)	Ru1–S2	2.307(3)
Fe1–Cp*1	1.762(2)	Ru1–Cp*2	1.8704(9)
Angles (°)			
S1–Fe1–S1A	106.48(11)	S1–Ru1–S2	85.80(8)
S1–Ru1–S1A	99.55(10)	S1–Ru1–Fe1	51.47(5)
S2–Ru1–Fe1	98.78(10)		
Torsion angles (°)			
S1–Fe1Ru1–S1A	154.78(12)		
Dihedral angle (°)			
Cp*1–Cp*2	62.14(44)		

Figure S4. ORTEP diagram of **3**

Thermal ellipsoids are shown at 50% probability level. All hydrogen atoms on carbons are omitted for the sake of clarity.

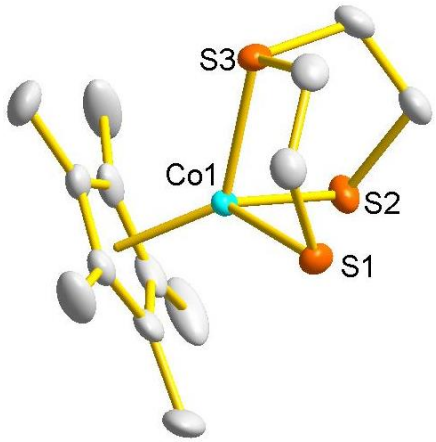

Table S10. Selected bond distances and angles for **3**

Distances (Å)			
Co1–S1	2.2474(7)	Co1–S3	2.2270(7)
Co1–S2	2.2465(7)	Co1–Cp*1	1.6934(3)
Angles (°)			
S1–Co1–S2	93.14(3)	S2–Co1–S3	90.34(3)
S1–Co1–S3	89.00(3)		

Figure S5. ORTEP diagram of **4a[BPh_4]**

Thermal ellipsoids are shown at 50% probability level. One BPh_4 anion and all hydrogen atoms on carbons are omitted for the sake of clarity.

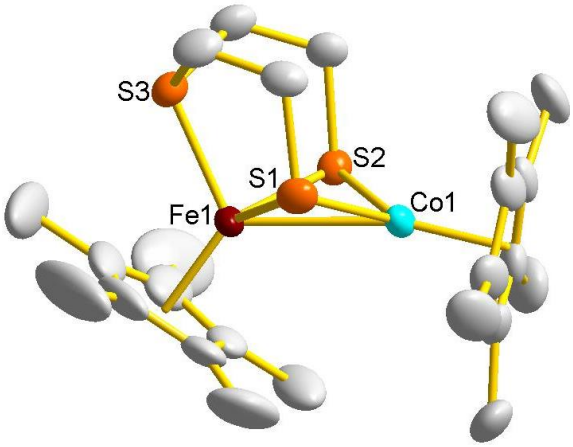

Table S11. Selected bond distances and angles for **4a[BPh_4]**

Distances (Å)			
Fe1–Co1	2.6772(8)	Fe1–Cp*1	1.7275(5)
Fe1–S1	2.213(1)	Co1–S1	2.177(1)
Fe1–S2	2.214(1)	Co1–S2	2.163(1)
Fe1–S3	2.236(1)	Co1–Cp*2	1.6967(5)
Angles (°)			
S1–Fe1–S2	94.21(5)	S1–Fe1–Co1	51.81(3)
S1–Fe1–S3	89.24(5)	S3–Fe1–Co1	113.18(4)
S2–Fe1–S3	89.40(5)	S2–Co1–Fe1	53.16(3)
S1–Co1–S2	96.74(5)		
Torsion angles (°)			
S1–Fe1Co1–S2	138.33(6)		
Dihedral angle (°)			
Cp*1–Cp*2	66.78(21)		

Figure S6. ORTEP diagram of **4b[BPh$_4$]**

Thermal ellipsoids are shown at 50% probability level. One BPh_4 anion and all hydrogen atoms on carbons except for the hydrogen atom on the Cp' ring are omitted for the sake of clarity.

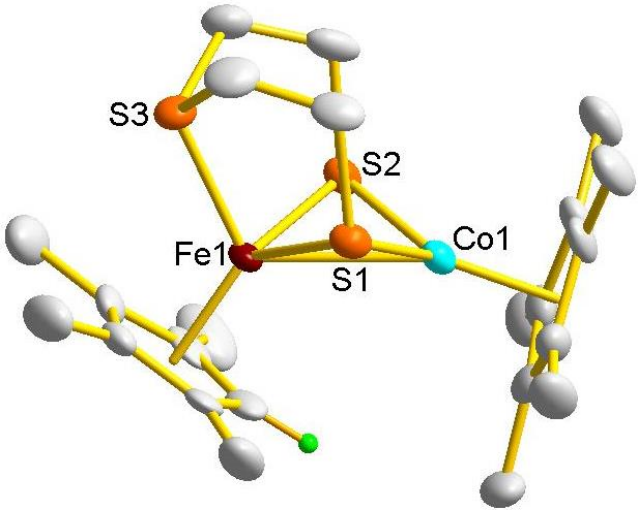

Table S12. Selected bond distances and angles for **4b[BPh$_4$]**

Distances (Å)			
Fe1–Co1	2.587(1)	Fe1–Cp*1	1.7211(6)
Fe1–S1	2.222(2)	Co1–S1	2.151(2)
Fe1–S2	2.213(2)	Co1–S2	2.168(2)
Fe1–S3	2.222(2)	Co1–Cp*2	1.6813(5)
Angles (°)			
S1–Fe1–S2	94.58(7)	S1–Fe1–Co1	52.48(5)
S1–Fe1–S3	89.11(7)	S3–Fe1–Co1	115.79(6)
S2–Fe1–S3	89.51(7)	S2–Co1–Fe1	53.01(5)
S1–Co1–S2	97.95(8)		
Torsion angles (°)			
S1–Fe1Co1–S2	134.77(6)		
Dihedral angle (°)			
Cp*1–Cp*2	73.18(19)		

Figure S7. ORTEP diagram of **7[PF$_6$]$_2$**

Thermal ellipsoids are shown at 50% probability level. Two PF_6 anions and all hydrogen atoms on carbons are omitted for the sake of clarity.

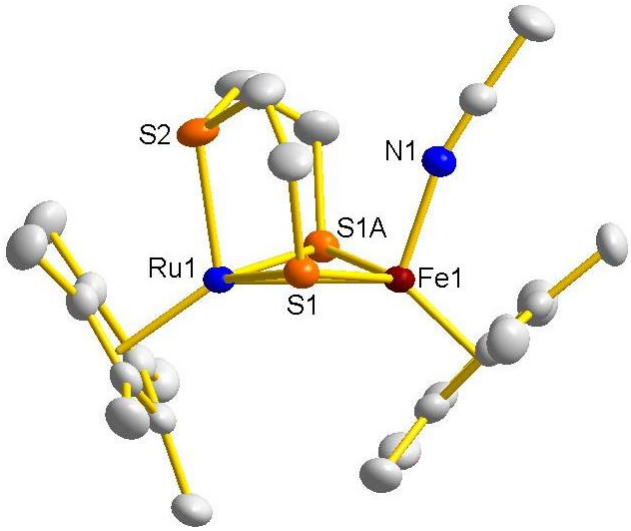

Table S13. Selected bond distances and angles for **7[PF$_6$]$_2$**

Distances (Å)			
Fe1–Ru1	2.794(2)	Ru1–S1	2.288(2)
Fe1–S1	2.240(2)	Ru1–S3	2.304(2)
Fe1–N1	1.934(8)	Ru1–Cp*2	1.9915(8)
Fe1–Cp*1	1.758(1)		
Angles (°)			
S1–Fe1–S1A	103.09(9)	S1–Ru1–S3	87.06(6)
S1–Fe1–N1	94.00(15)	S1–Ru1–S1A	100.13(8)
S3–Ru1–Fe1	97.59(8)	S1–Ru1–Fe1	51.13(4)
Torsion angles (°)			
S1–Fe1Ru1–S1A	159.89(4)		
Dihedral angle (°)			
Cp*1–Cp*2	76.76(19)		

Figure S8. ORTEP diagram of **8[PF_6]**

Thermal ellipsoids are shown at 50% probability level. One PF_6 anion and all hydrogen atoms on carbons are omitted for the sake of clarity.

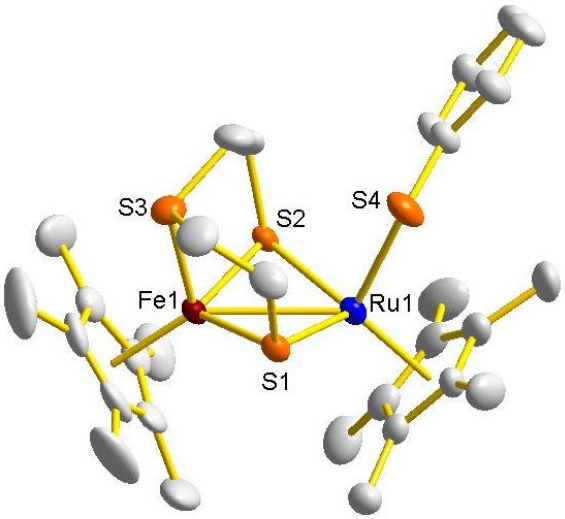

Table S14. Selected bond distances and angles for **8[PF_6]**

Distances (Å)			
Fe1–Ru1	2.8177(7)	Ru1–S1	2.306(1)
Fe1–S1	2.222(1)	Ru1–S2	2.314(1)
Fe1–S2	2.221(1)	Ru1–S4	2.385(1)
Fe1–S3	2.238(1)	Ru1–Cp*2	1.9052(3)
Fe1–Cp*1	1.7909(5)		
Angles (°)			
S1–Fe1–S2	102.41(4)	S3–Fe1–Ru1	103.82(4)
S1–Fe1–S3	88.35(5)	S1–Ru1–S2	97.12(4)
S2–Fe1–S3	88.93(5)	S1–Ru1–S4	92.66(4)
S1–Fe1–Ru1	52.86(3)	S2–Ru1–S4	95.85(4)
Torsion angles (°)			
S1–Fe1Ru1–S2	155.05(5)		
Dihedral angle (°)			
Cp*1–Cp*2	81.09(22)		

Figure S9. ORTEP diagram of **9[BPh$_4$]**

Thermal ellipsoids are shown at 50% probability level. One BPh_4 anion and all hydrogen atoms except for the terminal hydride are omitted for the sake of clarity.

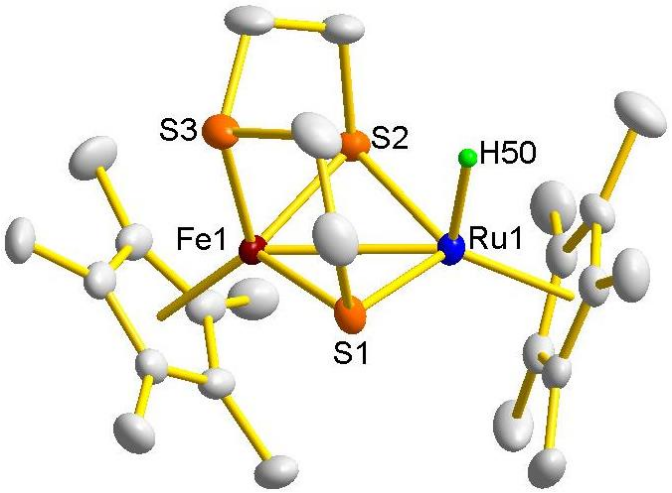

Table S15. Selected bond distances and angles for **9[BPh$_4$]**

Distances (Å)			
Fe1–Ru1	2.7411(4)	Ru1–S1	2.2420(7)
Fe1–S1	2.2404(7)	Ru1–S2	2.2680(7)
Fe1–S2	2.2530(7)	Ru1–H50	1.626(29)
Fe1–S3	2.2528(8)	Ru1–Cp*2	1.8581(4)
Fe1–Cp*1	1.7577(5)		
Angles (°)			
S1–Fe1–S2	102.41(3)	S3–Fe1–Ru1	100.44(2)
S1–Fe1–S3	87.59(3)	S1–Ru1–S2	101.89(3)
S2–Fe1–S3	87.52(3)	S1–Ru1–Fe1	52.27(2)
S1–Fe1–Ru1	52.33(2)	S2–Ru1–Fe1	52.43(2)
Torsion angles (°)			
S1–Fe1Ru1–S2	157.47(6)		
Dihedral angle (°)			
Cp*1–Cp*2	66.29(18)		

VI. ESI-HRMS

Figure S10. ESI-HRMS of **2[PF$_6$]** in THF

(a) The signal at an *m/z* = 580.0549 corresponds to **2**$^+$. (b) Calculated isotopic distribution for **2**$^+$ (upper) and the amplifying experimental diagram for **2**$^+$ (bottom).

(a)

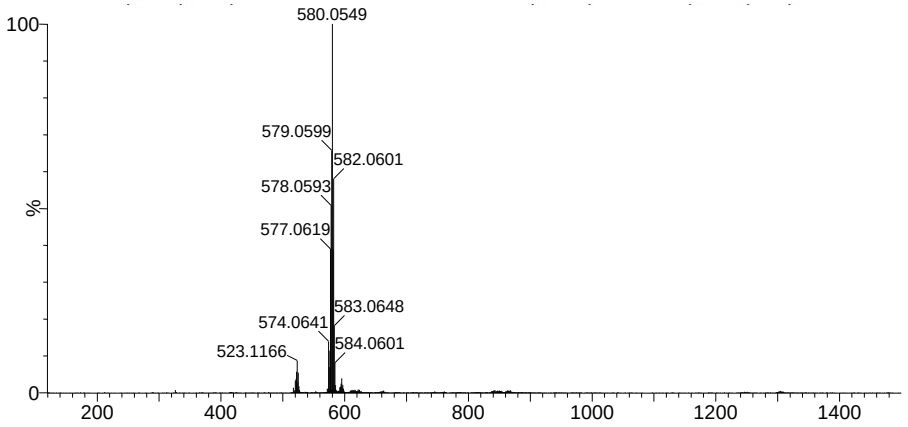

(b)

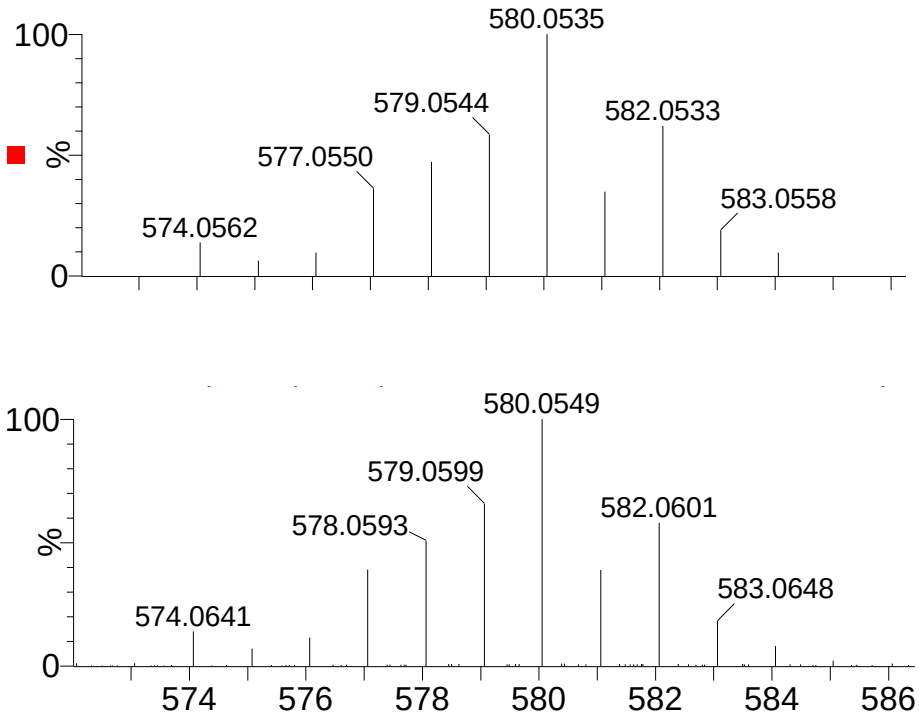

Figure S11. ESI-HRMS of **4a[BPh$_4$]** in THF

(a) The signal at an *m/z* = 537.0803 corresponds to **4a**$^+$. (b) Calculated isotopic distribution for **4a**$^+$ (upper) and the amplifying experimental diagram for **4a**$^+$ (bottom).

(a)

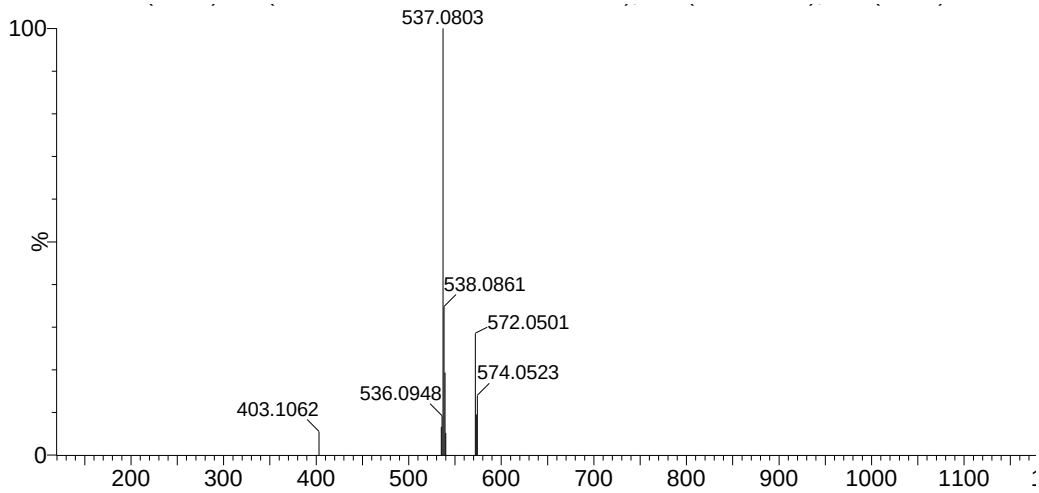

(b)

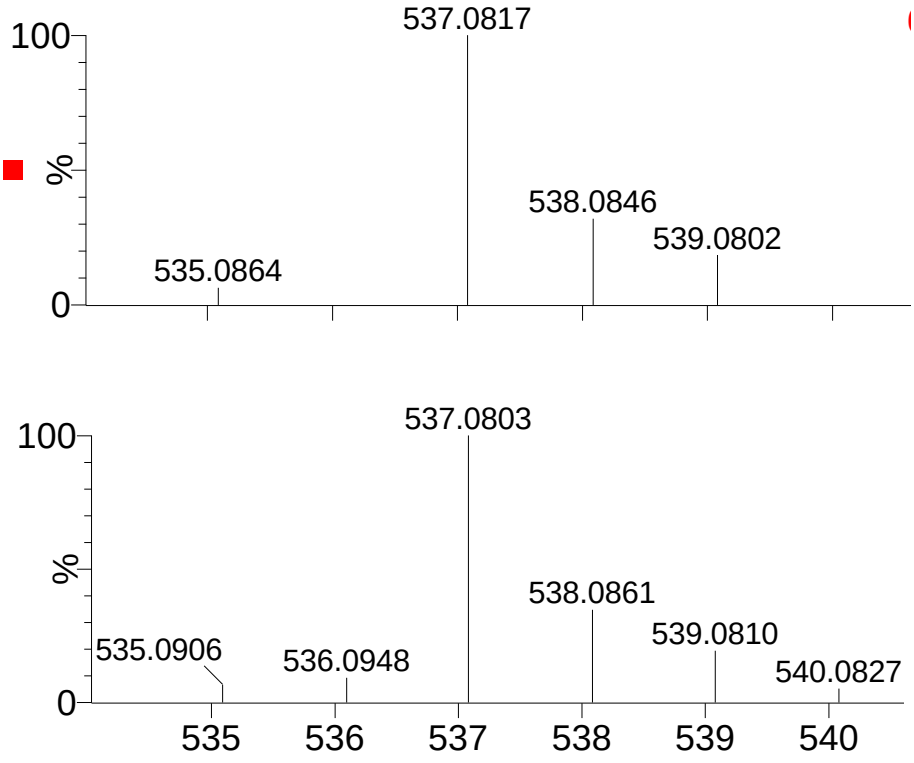

Figure S12. ESI-HRMS of **4b[BPh$_4$]** in THF

(a) The signal at an *m/z* = 523.0658 corresponds to **4b**$^+$. (b) Calculated isotopic distribution for **4b**$^+$ (upper) and the amplifying experimental diagram for **4b**$^+$ (bottom).

(a)

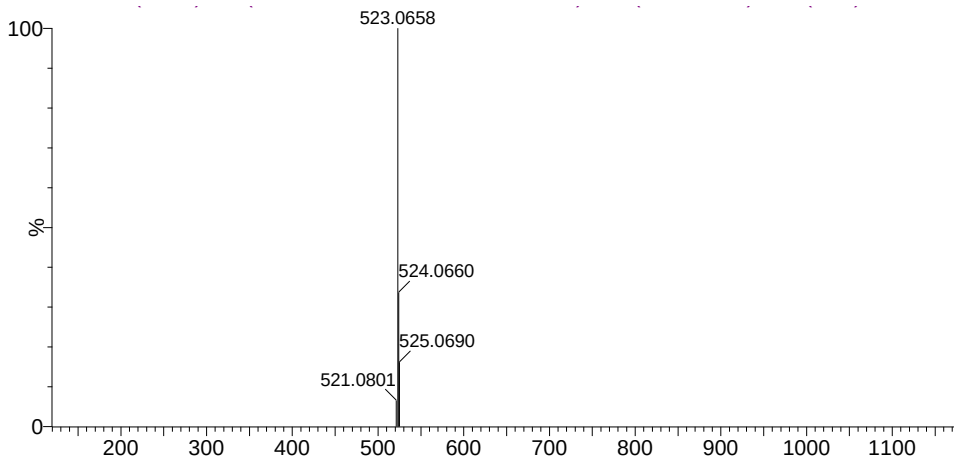

(b)

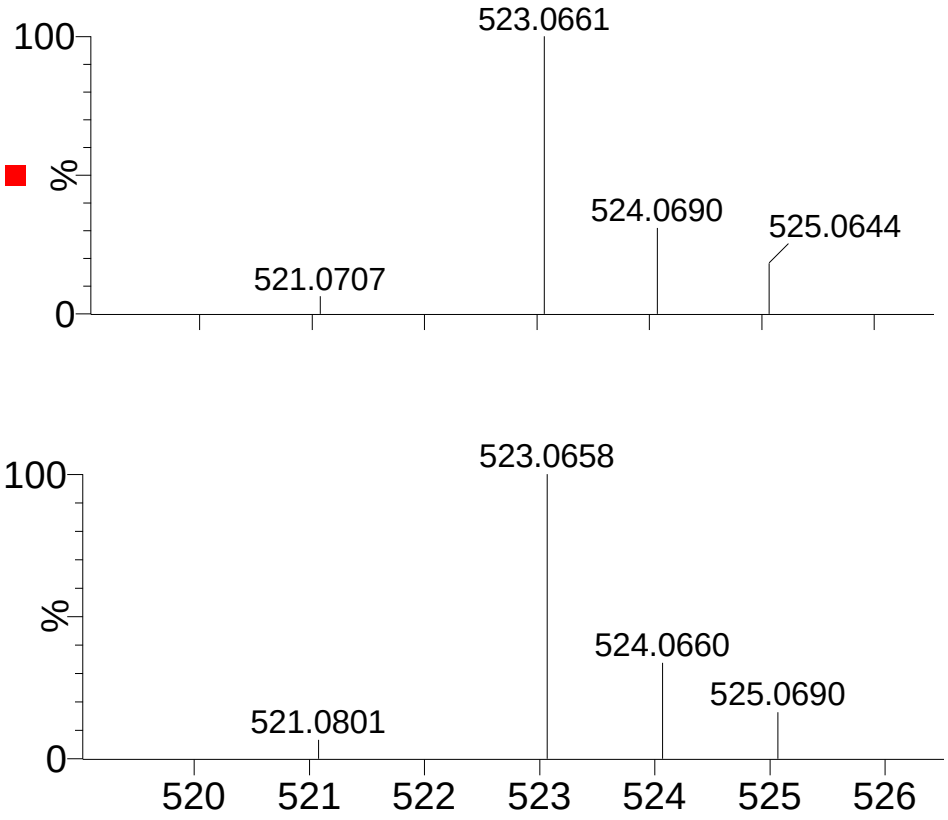

Figure S13. ESI-HRMS of **7[PF$_6$]$_2$** in MeCN

(a) The signal at an *m/z* = 290.0259 corresponds to **7**$^{2+}$. (b) Calculated isotopic distribution for **7**$^{2+}$ (upper) and the amplifying experimental diagram for **7**$^{2+}$ (bottom).

(a)

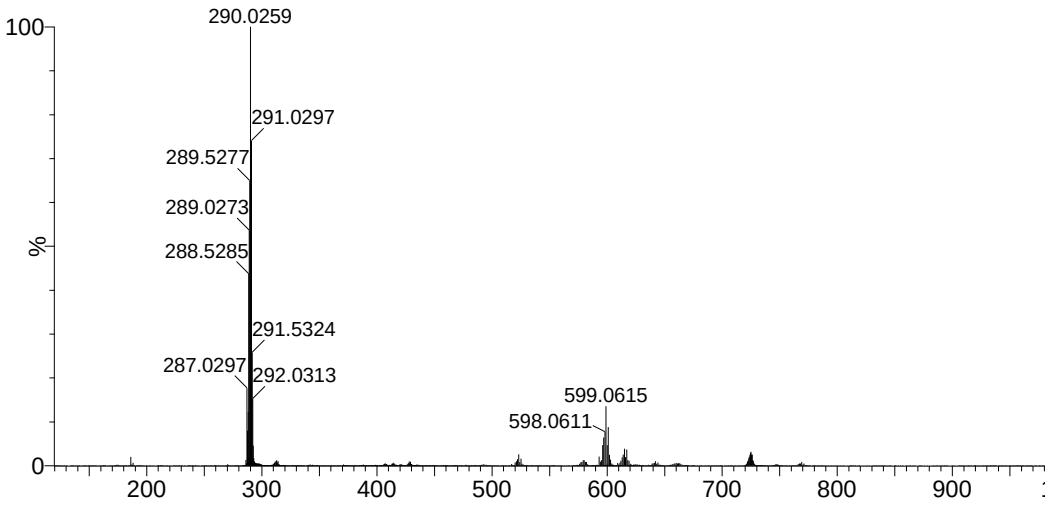

(b)

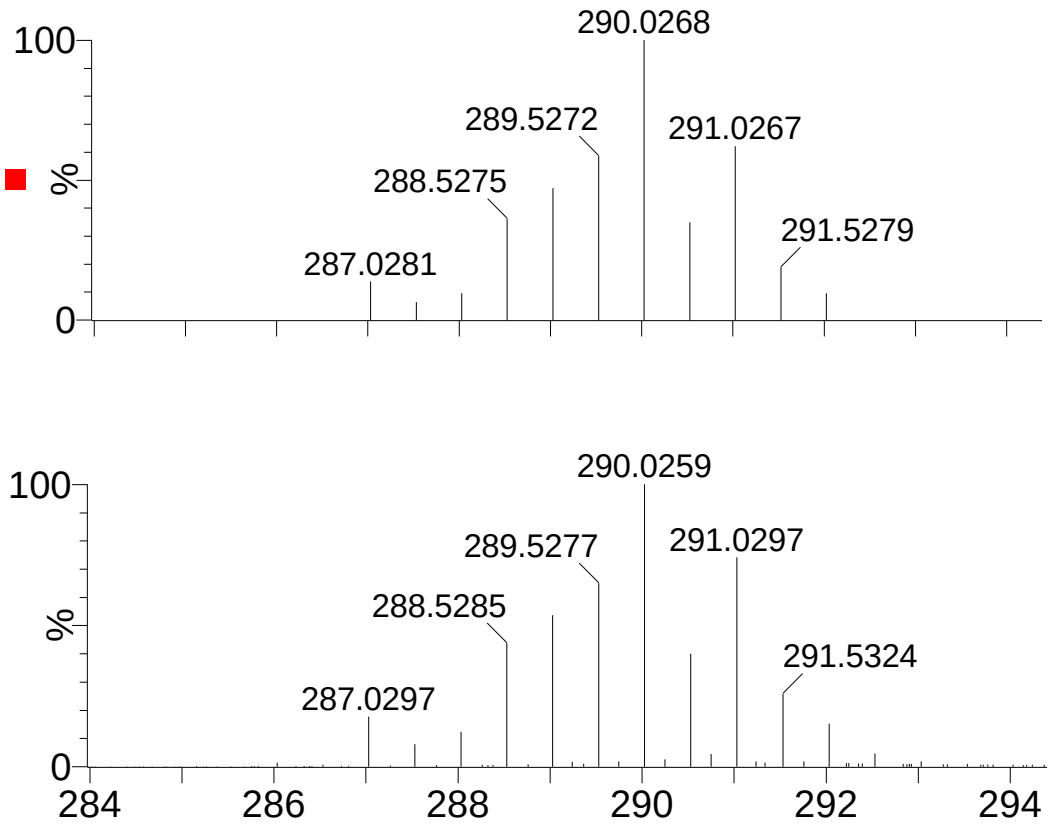

Figure S14. ESI-HRMS of **8[PF$_6$]** in THF

(a) The signal at an *m/z* = 689.0656 corresponds to **8**$^+$. (b) Calculated isotopic distribution for **8**$^+$ (upper) and the amplifying experimental diagram for **8**$^+$ (bottom).

(a)

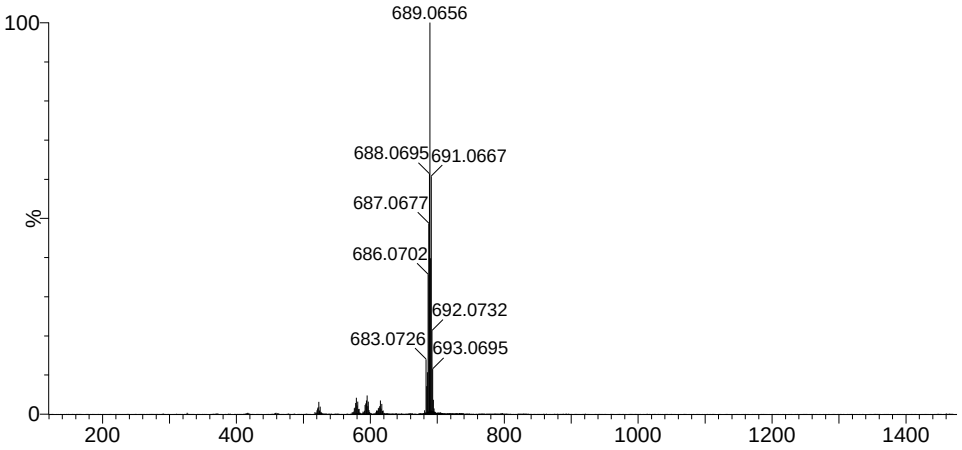

(b)

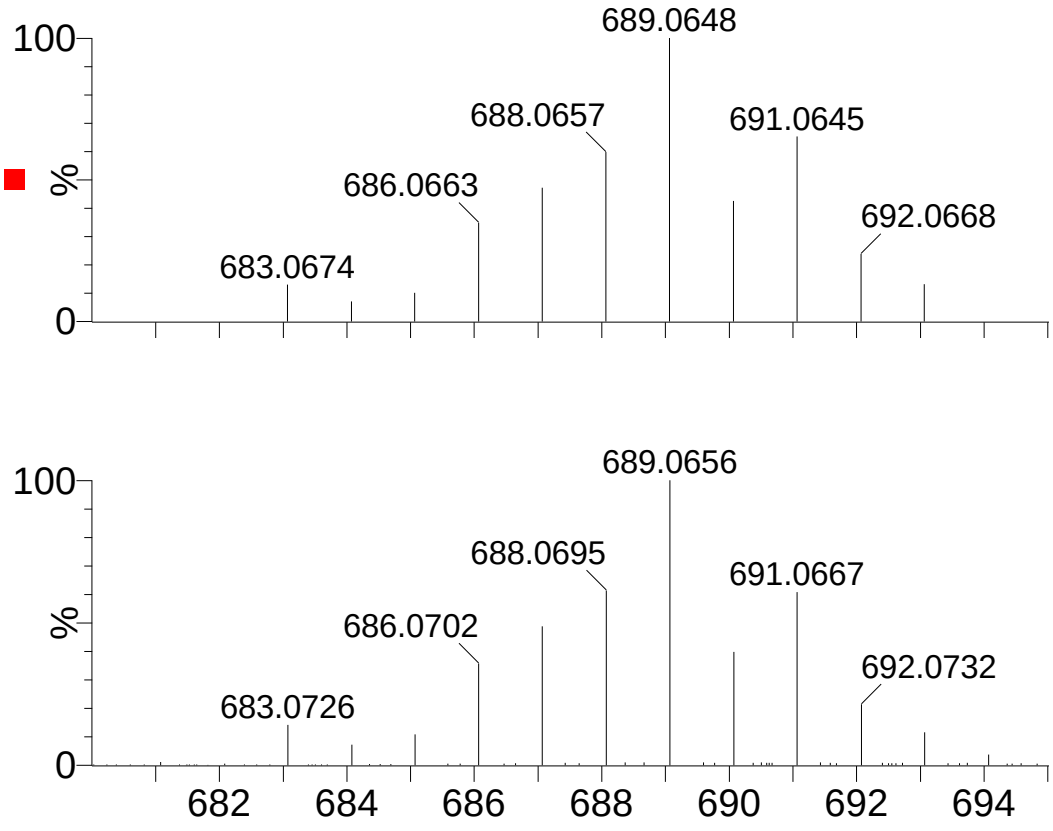

Figure S15. ESI-HRMS of **9[BPh$_4$]** in THF

(a) The signal at an *m/z* = 581.0615 corresponds to **9**$^+$. (b) Calculated isotopic distribution for **9**$^+$ (upper) and the amplifying experimental diagram for **9**$^+$ (bottom).

(a)

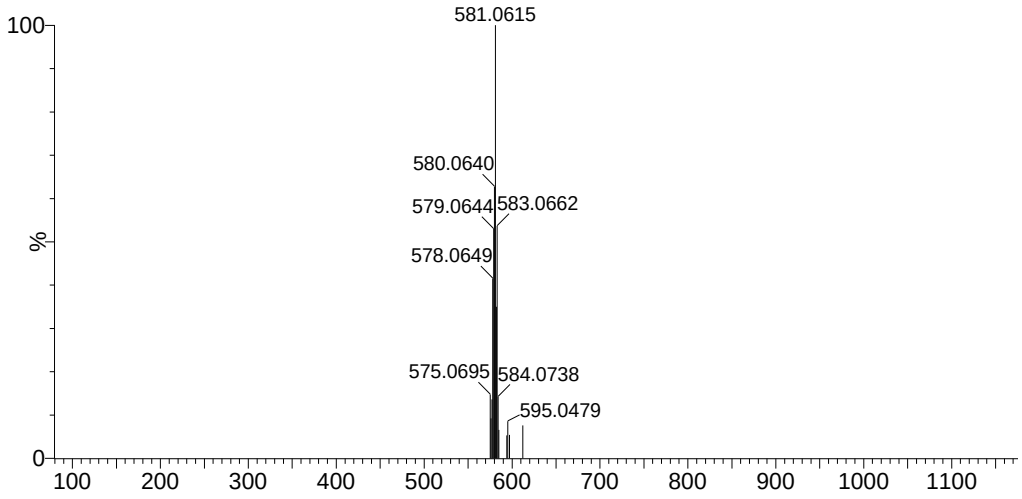

(b)

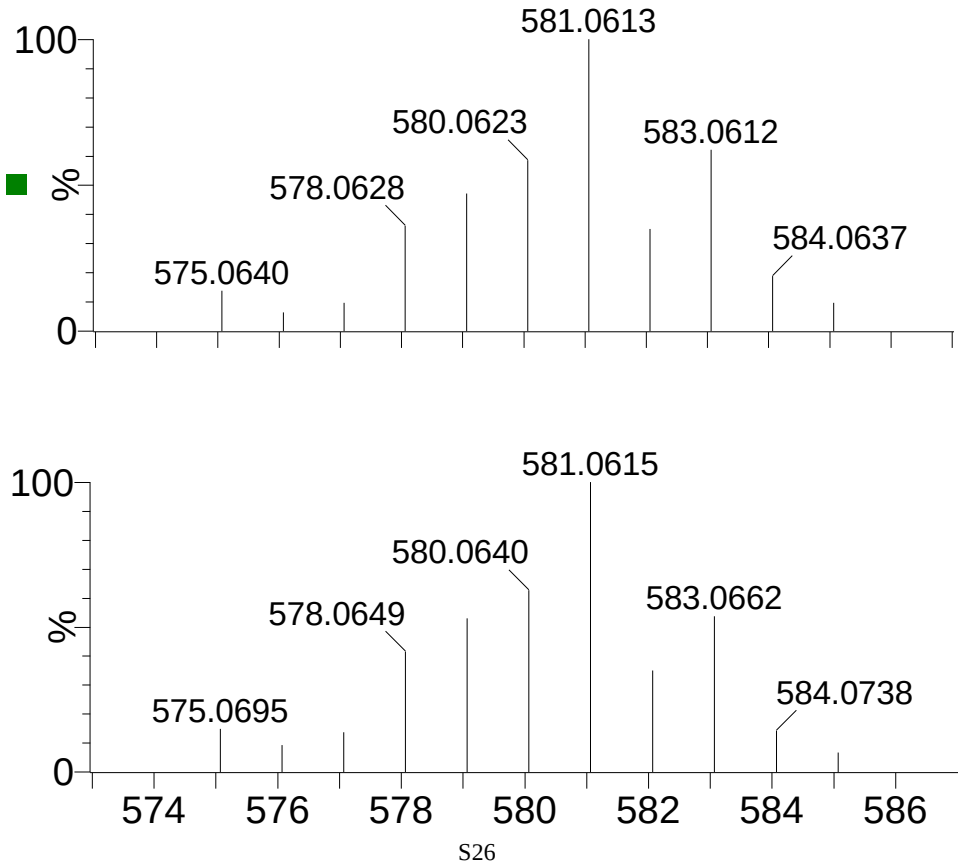

Figure S16. ESI-MS of the reaction of **2[PF_6]** with thiophenol in THF

The signals at *m/z* = 581.0613 and 689.0648 correspond to $\mathbf{9}^+$ and $\mathbf{8}^+$, respectively.

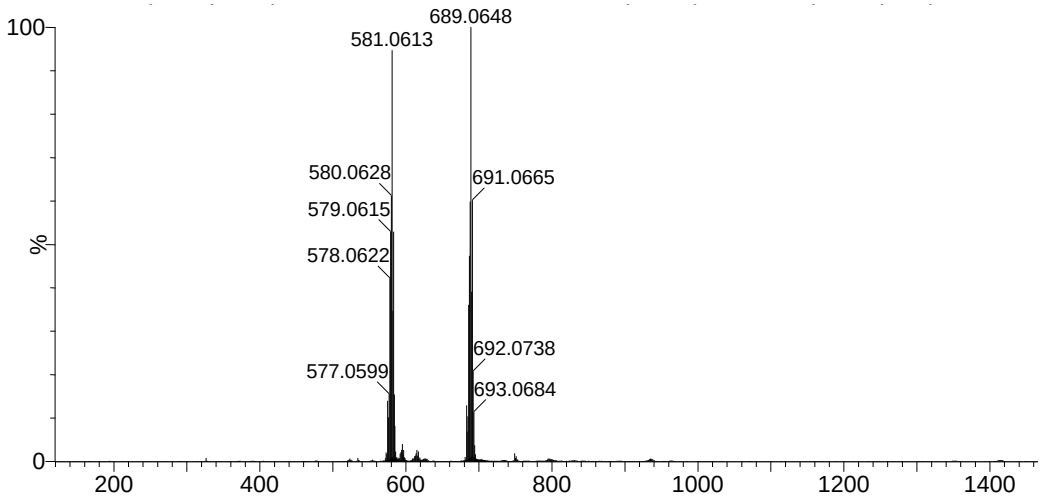

VII. NMR Spectra

Figure S17. The ^{1}H NMR spectrum of **2[PF$_6$]** in CD_3CN

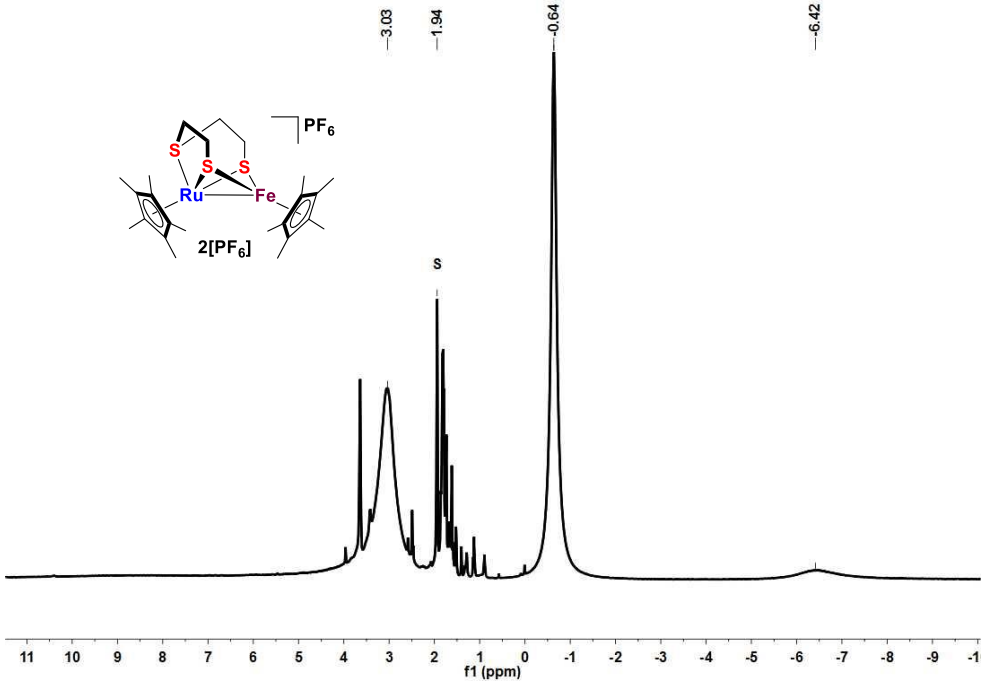

Figure S18. The ^{1}H NMR spectrum of the reaction of **2[PF$_6$]** and thiophenol in THF-d_8

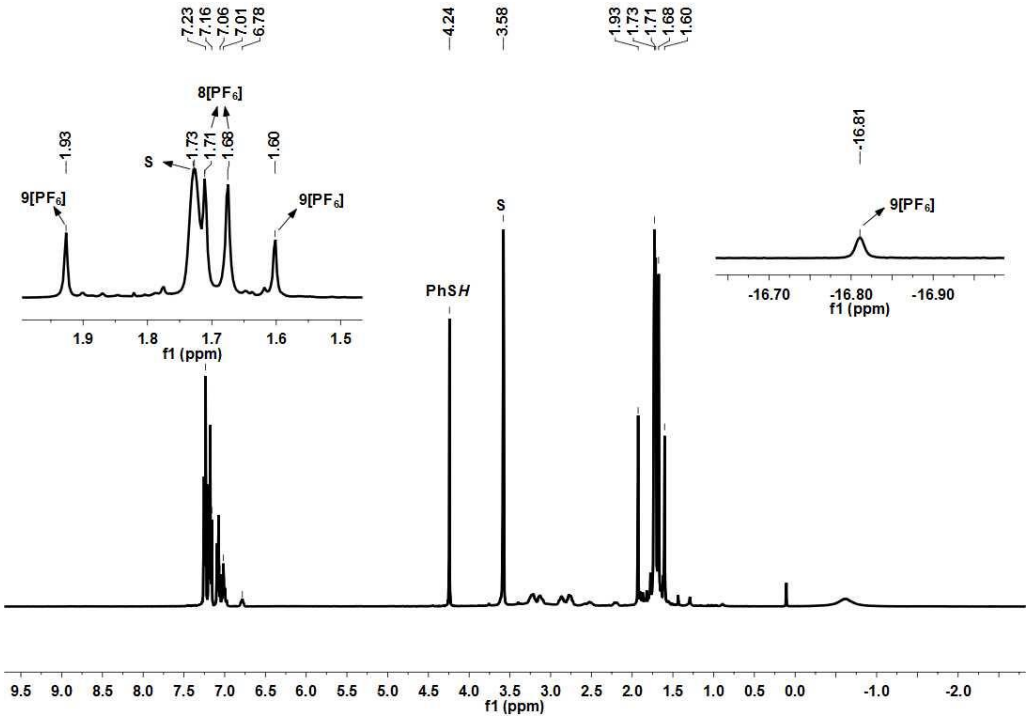

Figure S19. The ^{1}H NMR spectrum of **3** in C_6D_6

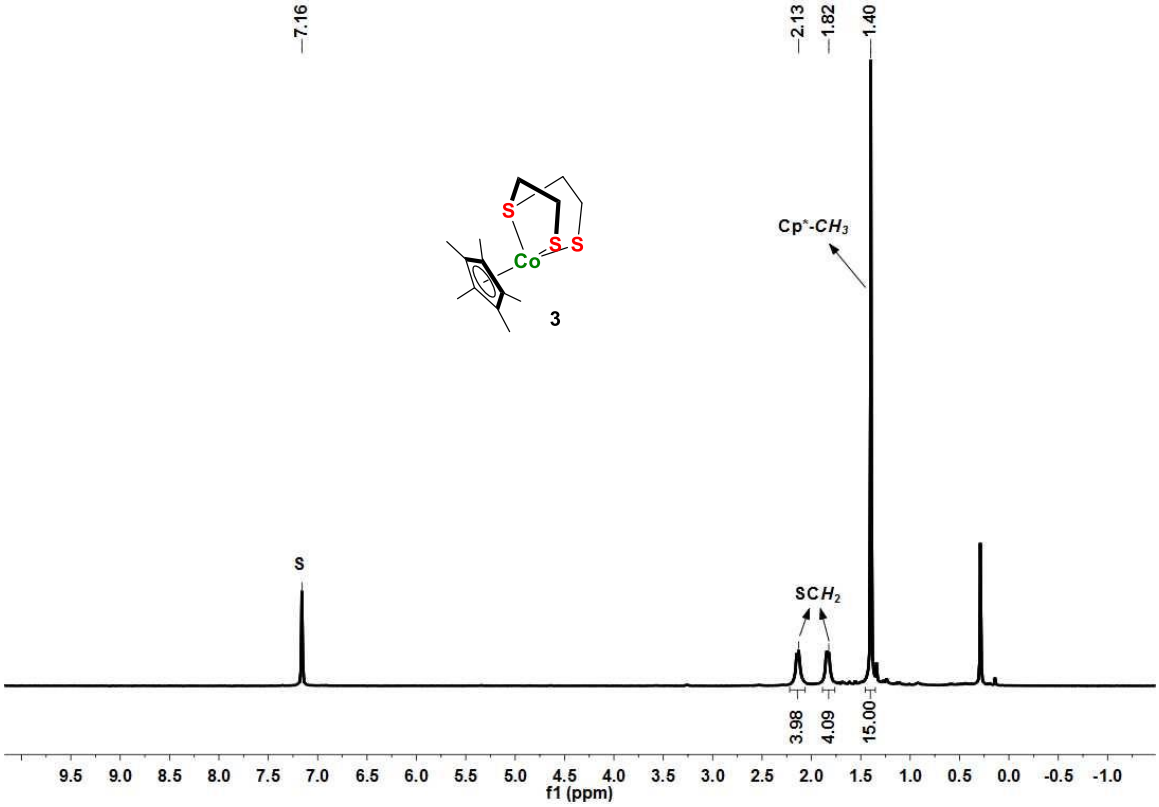

Figure S20. The ^{13}C NMR spectrum of **3** in C_6D_6

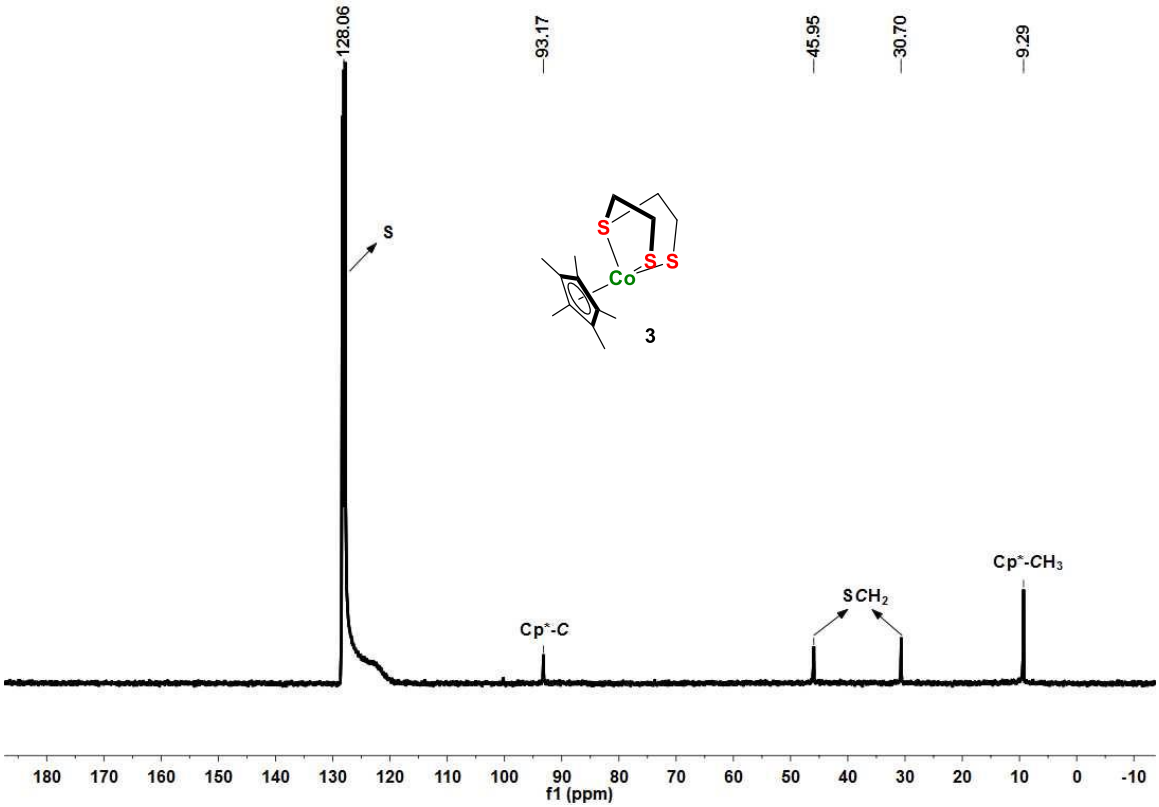

Figure S21. The ^{1}H NMR spectrum of **4a[BPh$_4$]** in CD_2Cl_2

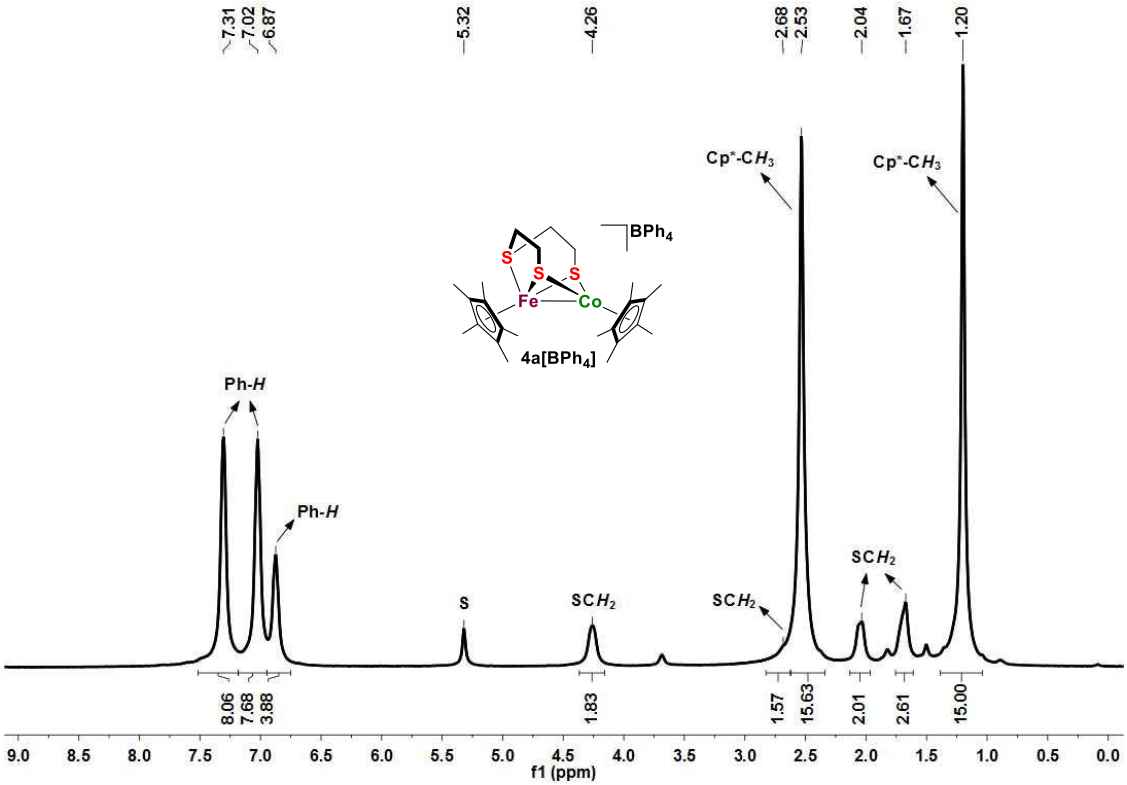

Figure S22. The ^{13}C NMR spectrum of **4a[BPh$_4$]** in CD_2Cl_2

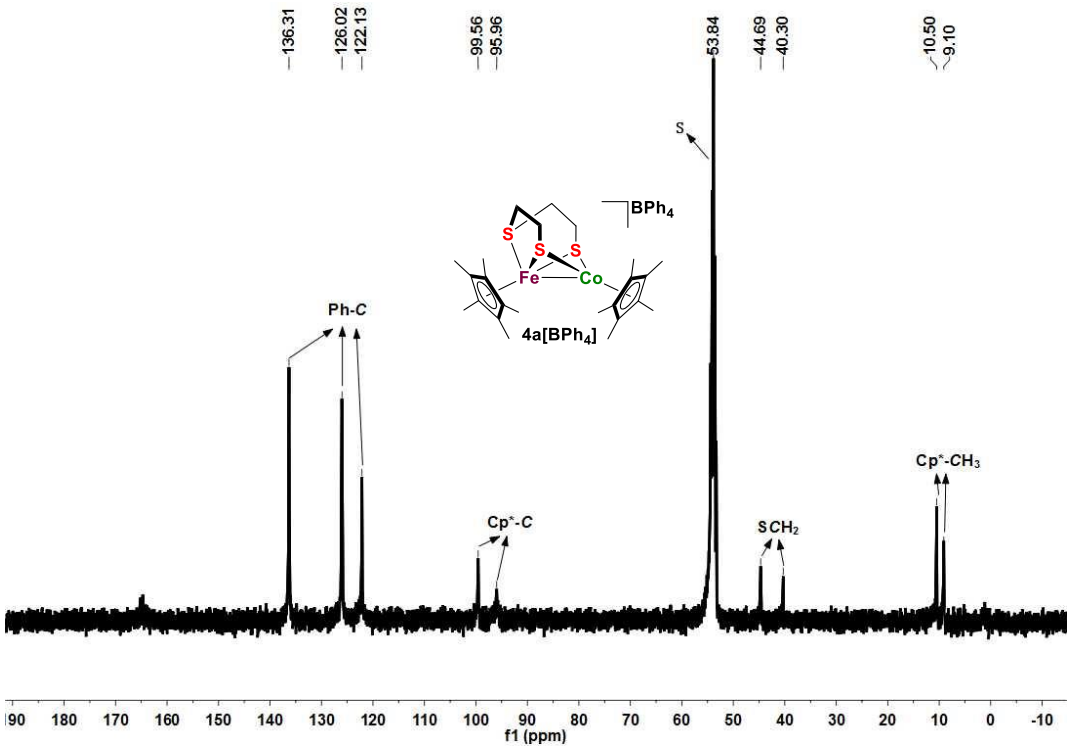

Figure S23. The ^{1}H NMR spectrum of **4b[BPh$_4$]** in CD_2Cl_2

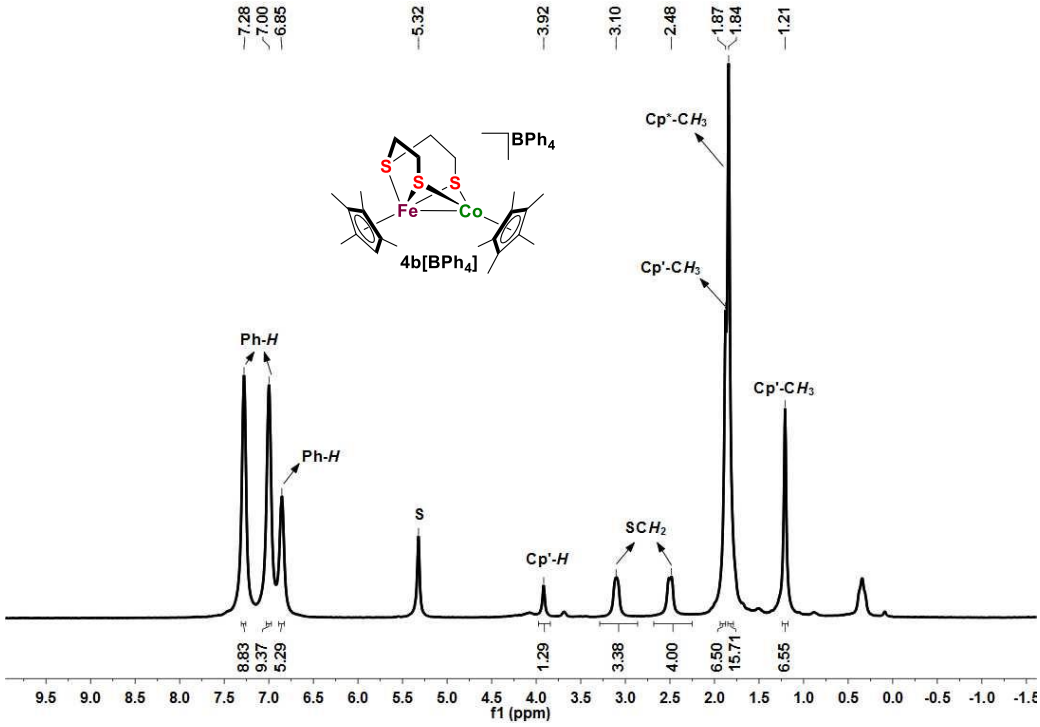

Figure S24. The ^{13}C NMR spectrum of **4b[BPh$_4$]** in CD_2Cl_2

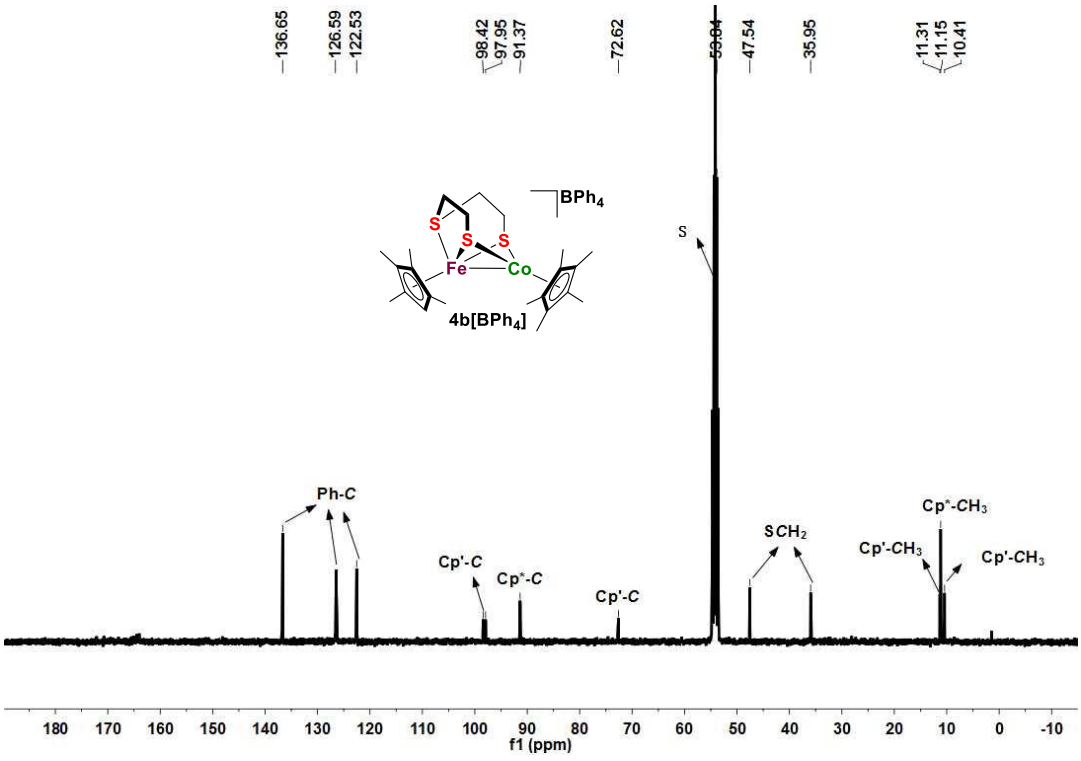

Figure S25. The ^{1}H NMR spectrum of **7[PF$_6$]$_2$** in CD_3CN

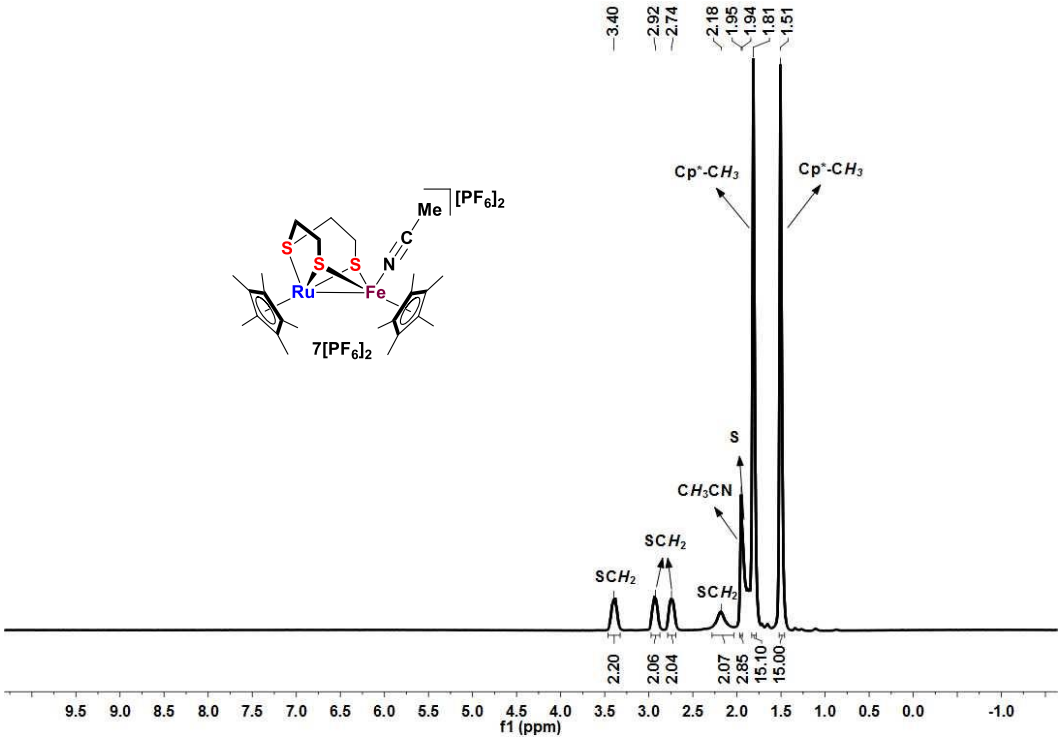

Figure S26. The ^{13}C NMR spectrum of **7[PF$_6$]$_2$** in CD_3CN

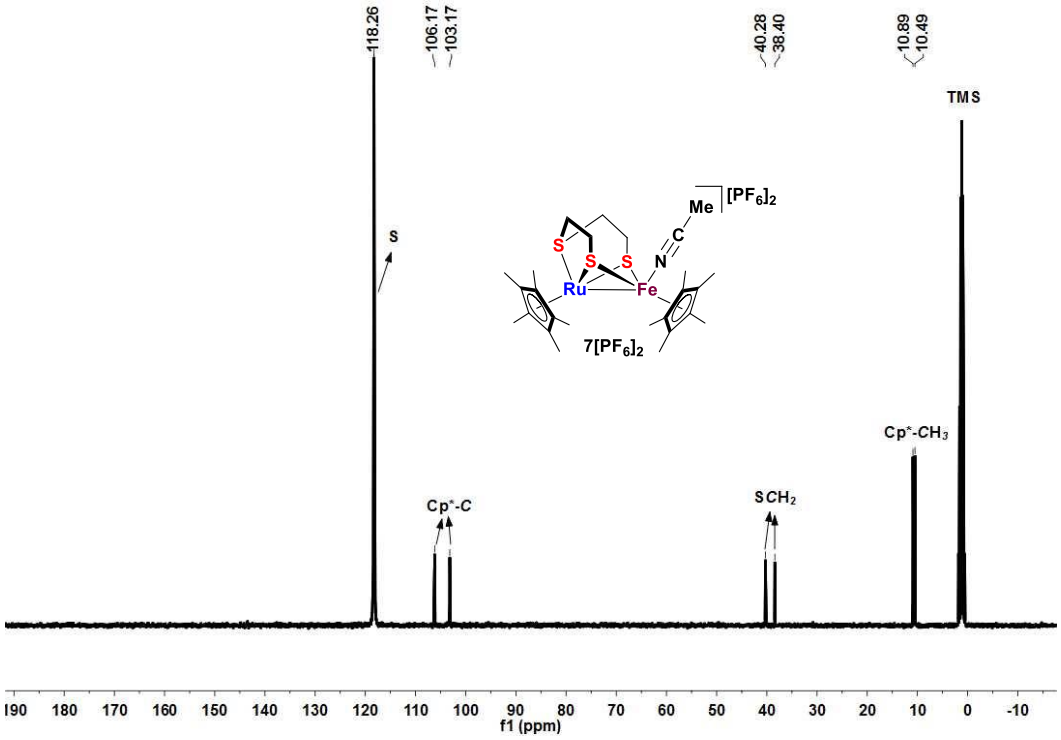

Figure S27. The ^{1}H NMR spectrum of **8[PF$_6$]** in CD_3CN

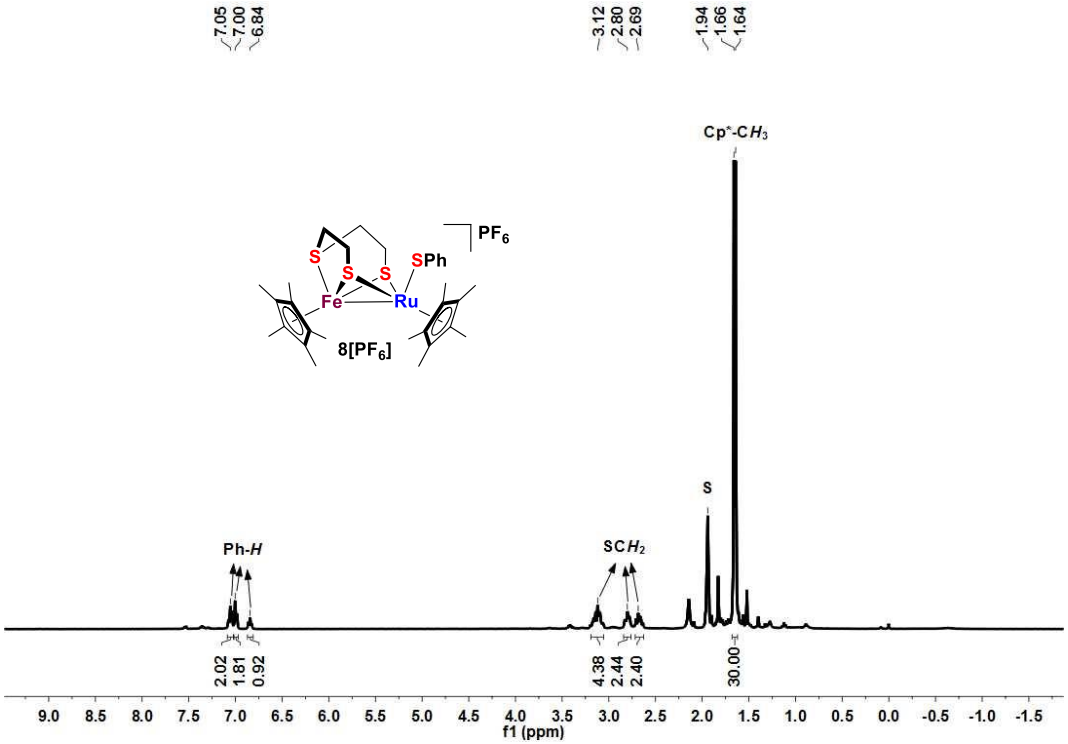

Figure S28. The ^{13}C NMR spectrum of **8[PF$_6$]** in CD_3CN

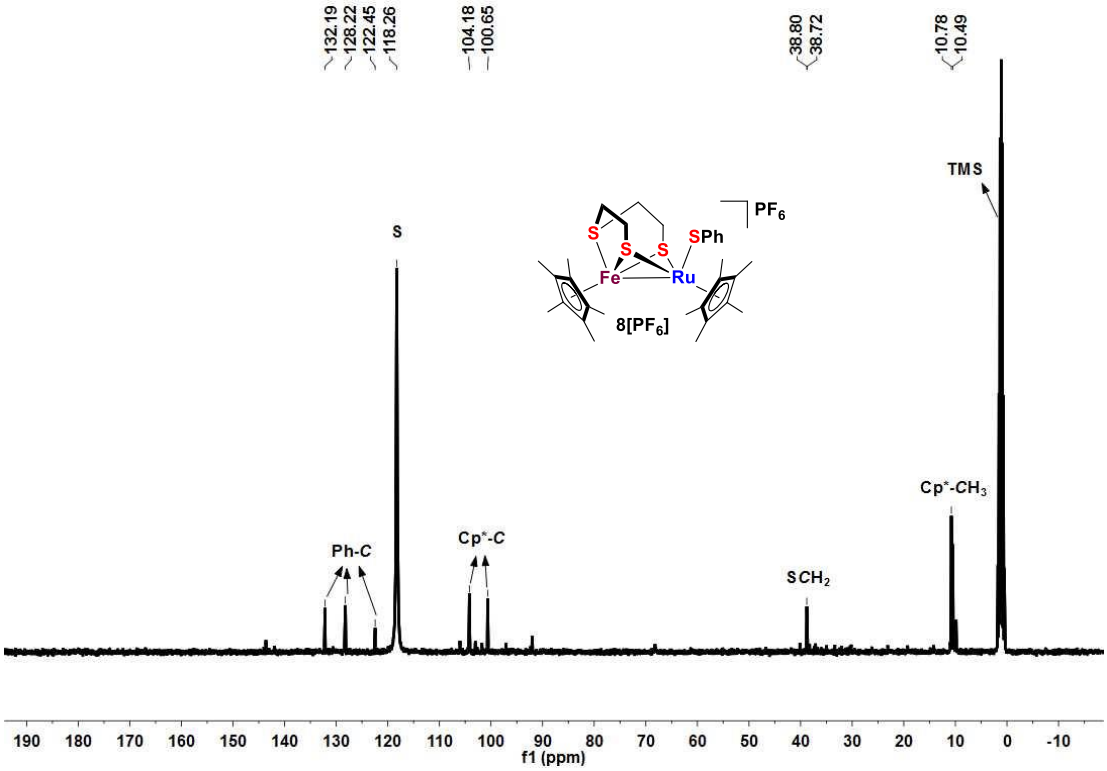

Figure S29. The ^{1}H NMR spectrum of **9[BPh$_4$]** in CD_3CN

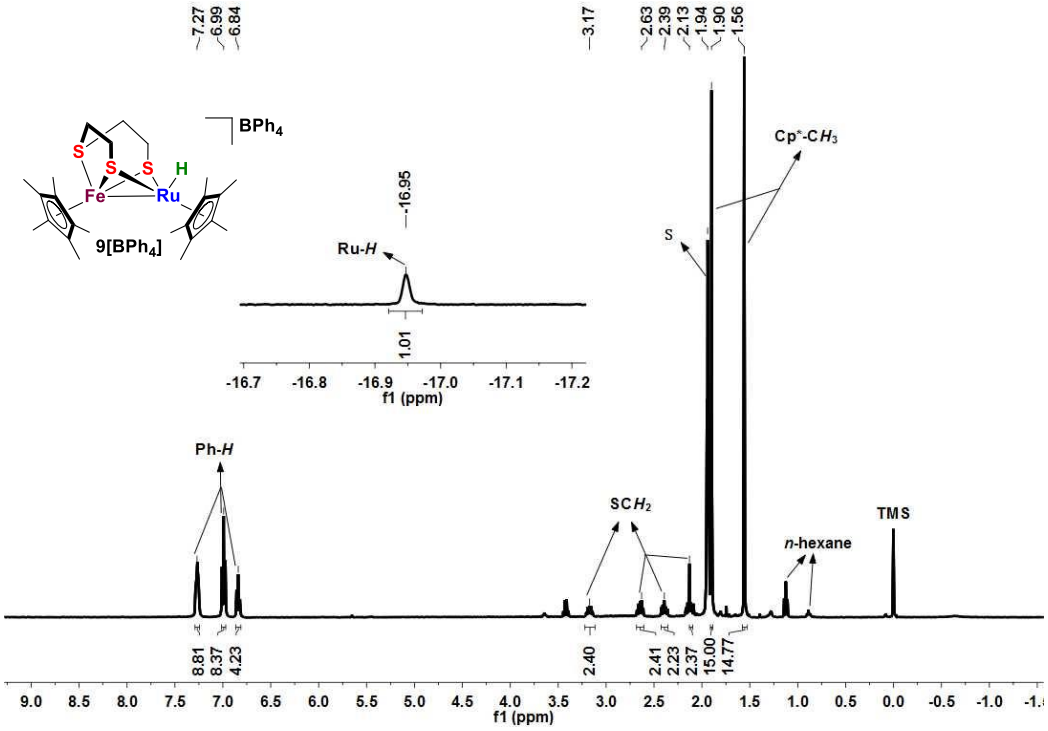

Figure S30. The ^{13}C NMR spectrum of **9[BPh$_4$]** in CD_3CN

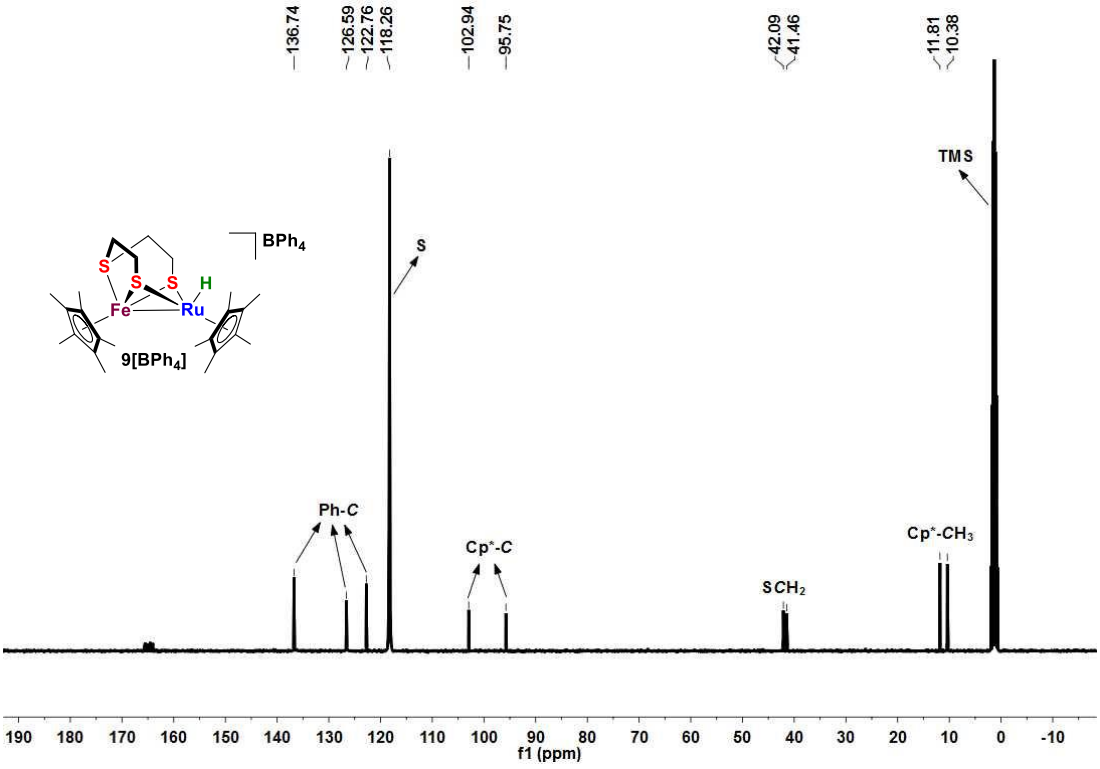

Figure S31. The ^{1}H NMR spectrum of **6a** in $CDCl_3$

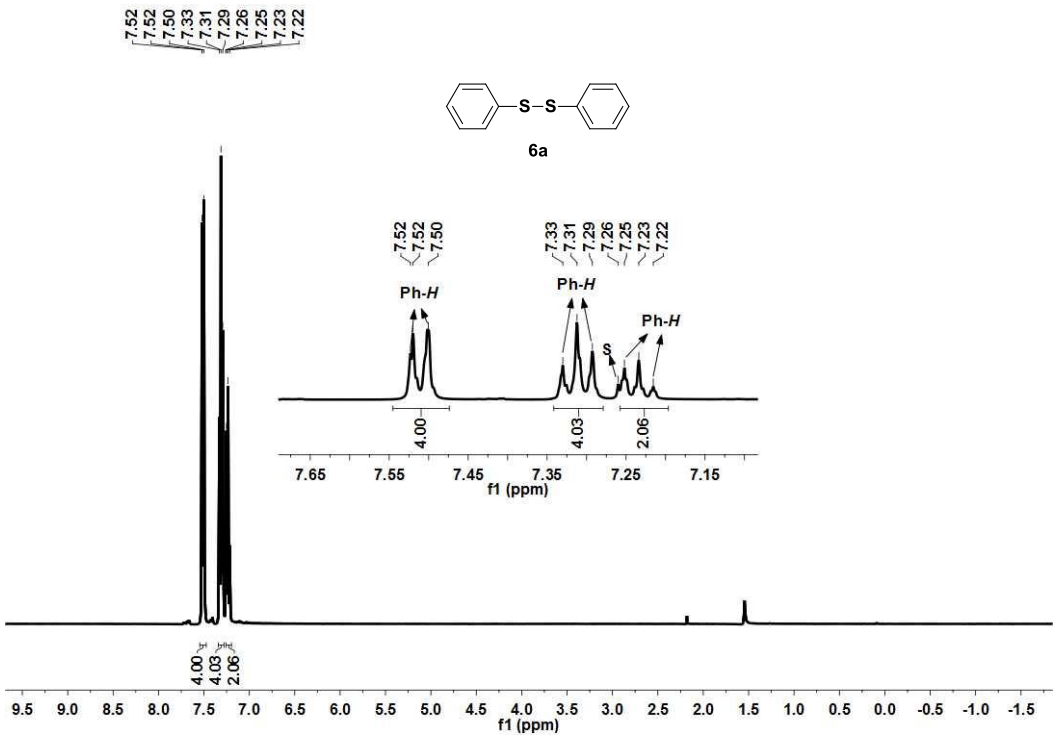

Figure S32. The ^{13}C NMR spectrum of **6a** in $CDCl_3$

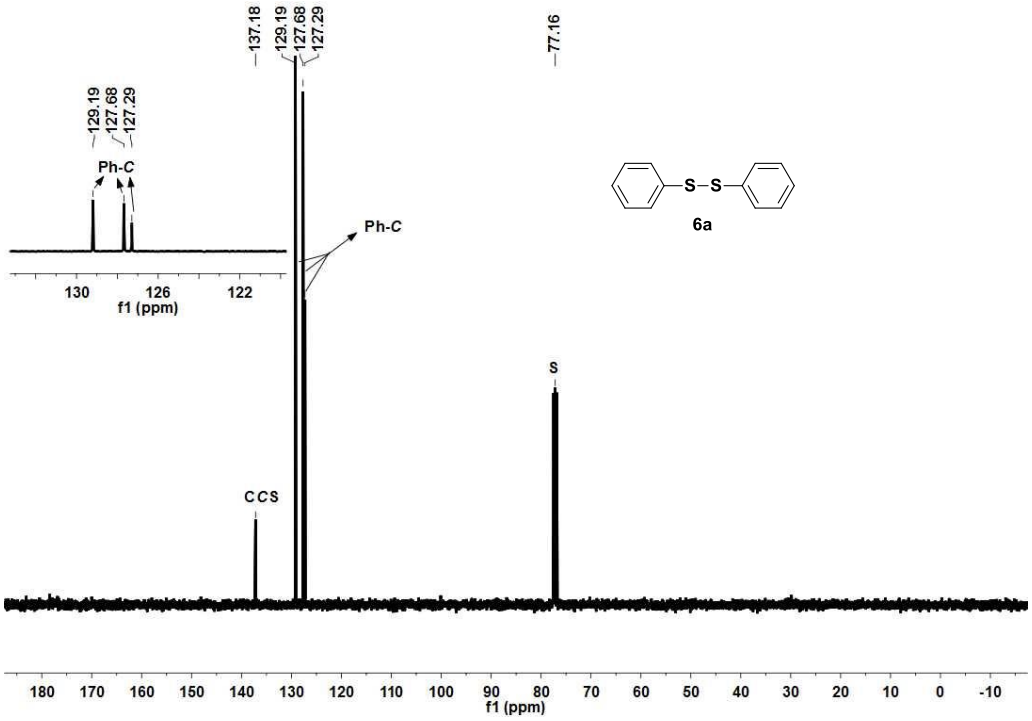

Figure S33. The ^{1}H NMR spectrum of **6b** in $CDCl_3$

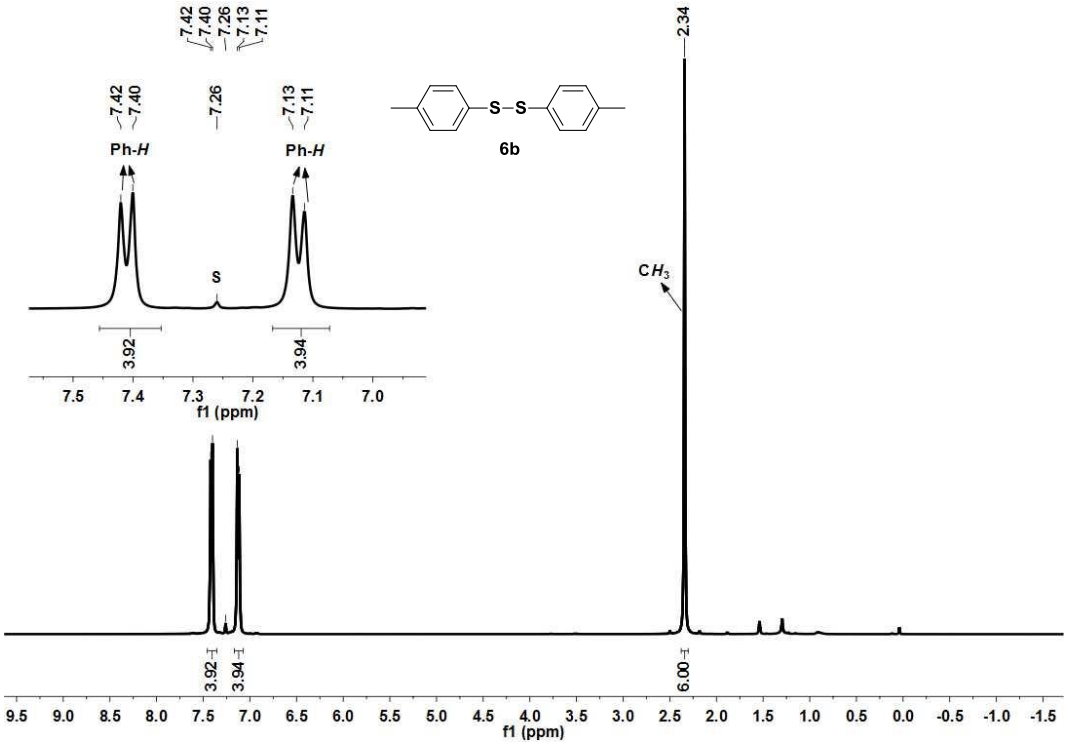

Figure S34. The ^{13}C NMR spectrum of **6b** in $CDCl_3$

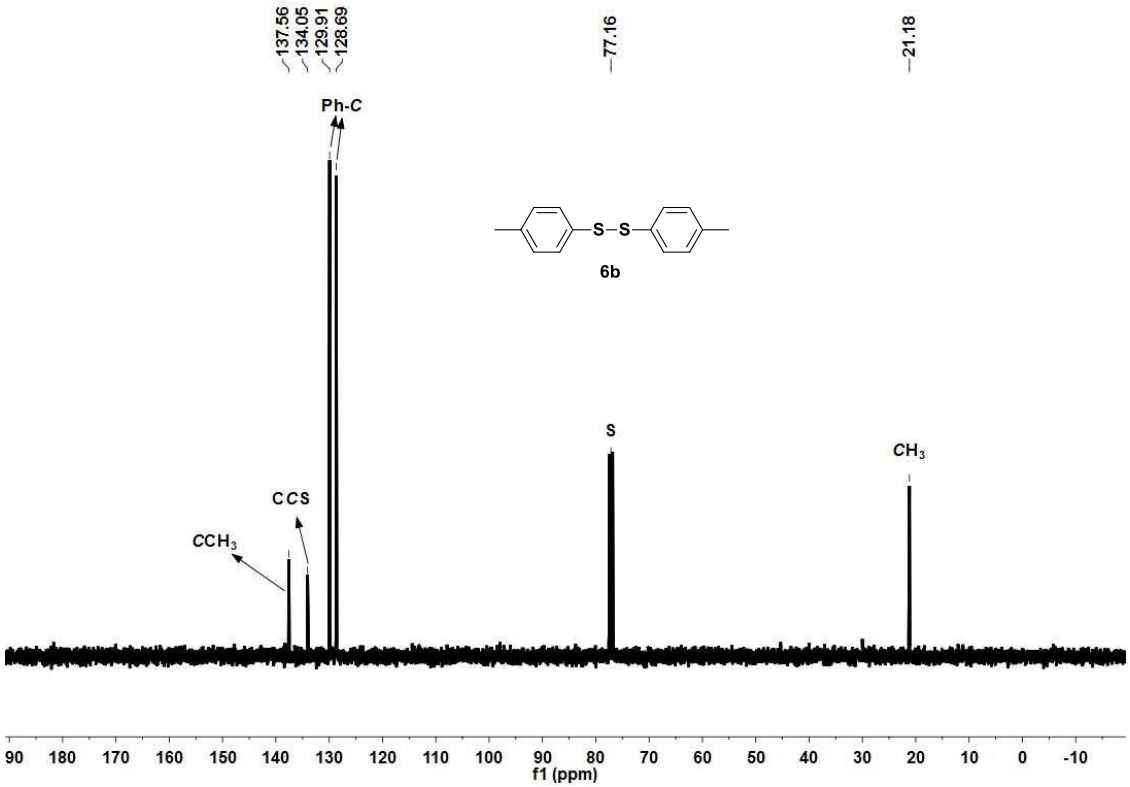

Figure S35. The ^{1}H NMR spectrum of **6c** in $CDCl_3$

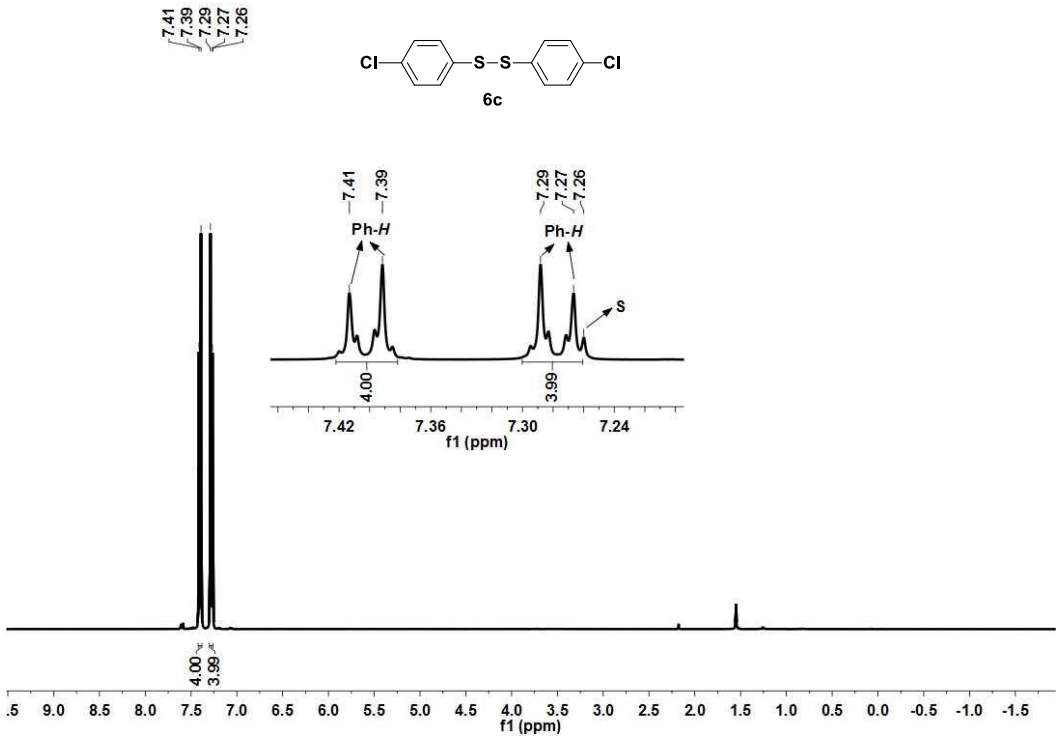

Figure S36. The ^{13}C NMR spectrum of **6c** in $CDCl_3$

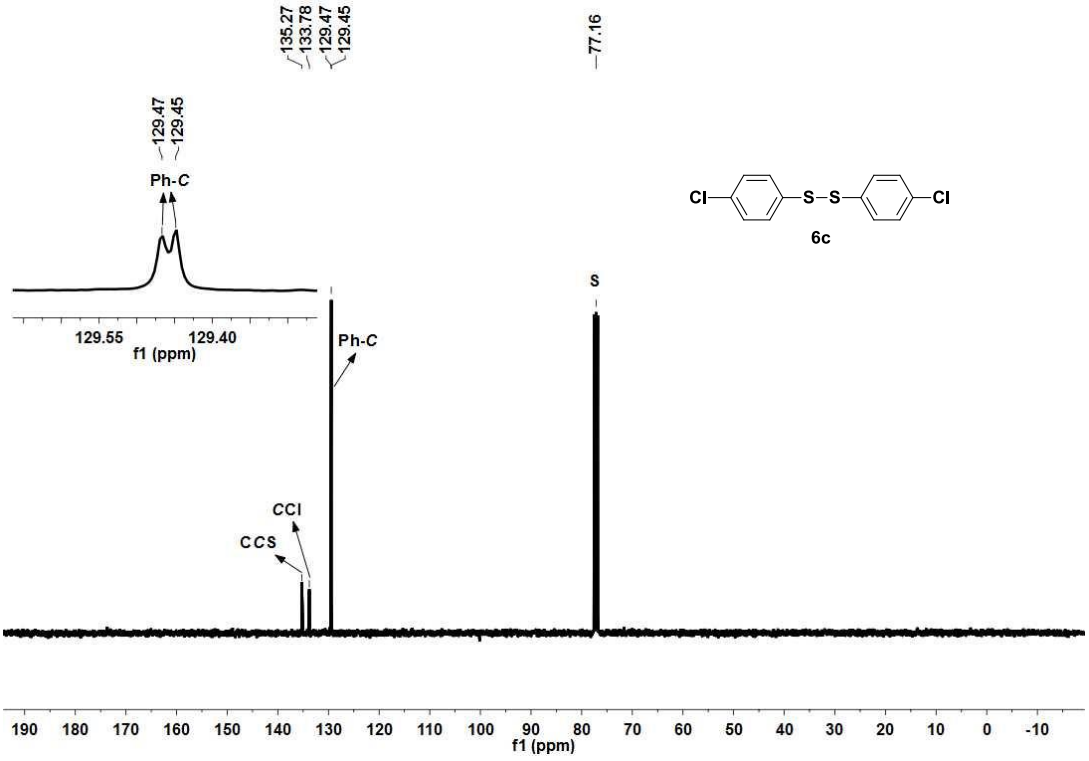

Figure S37. The ^{1}H NMR spectrum of **6d** in $CDCl_3$

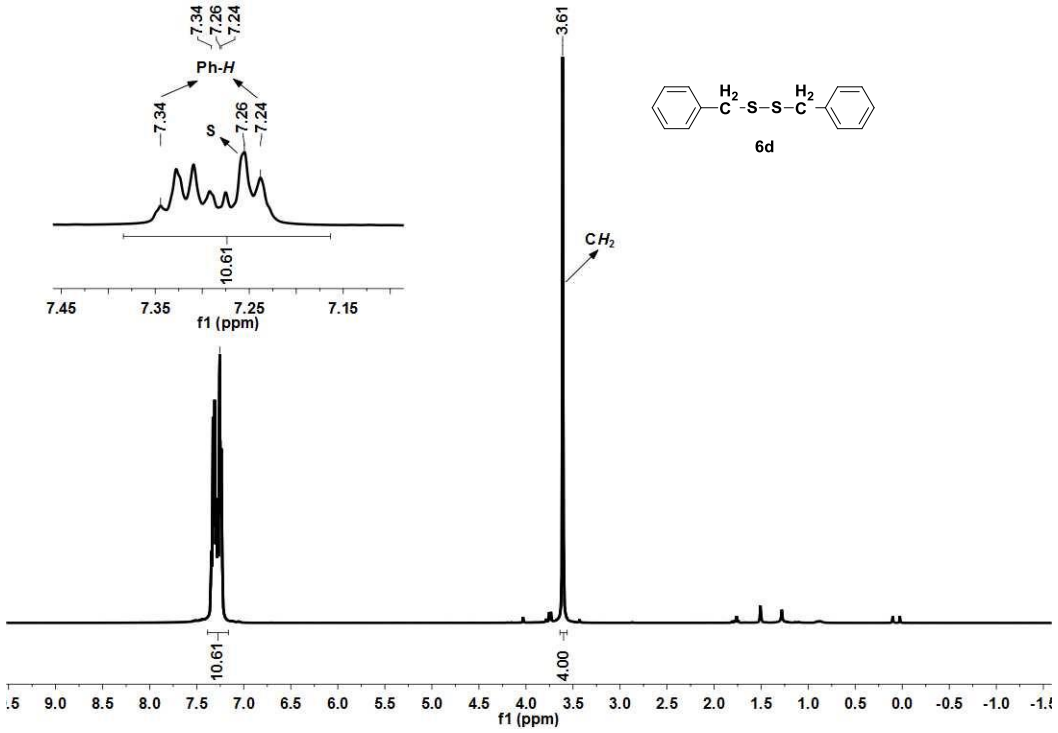

Figure S38. The ^{13}C NMR spectrum of **6d** in $CDCl_3$

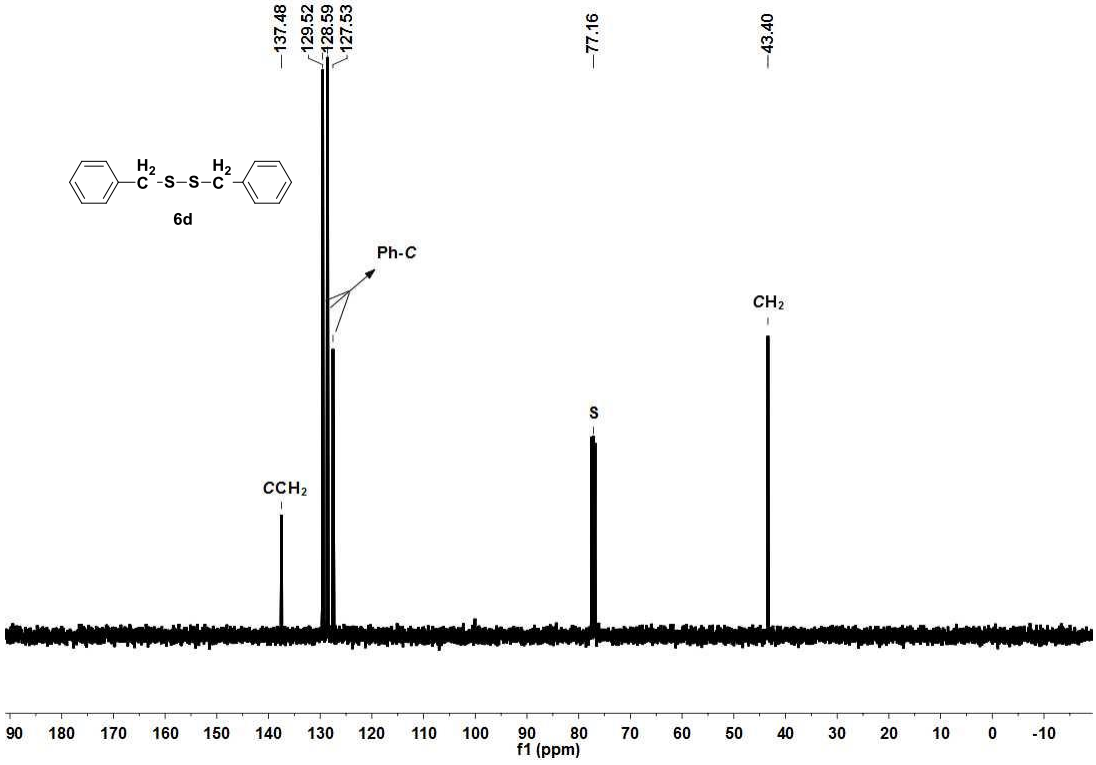

Figure S39. The ^{1}H NMR spectrum of **6e** in D_2O (4% NaOD)

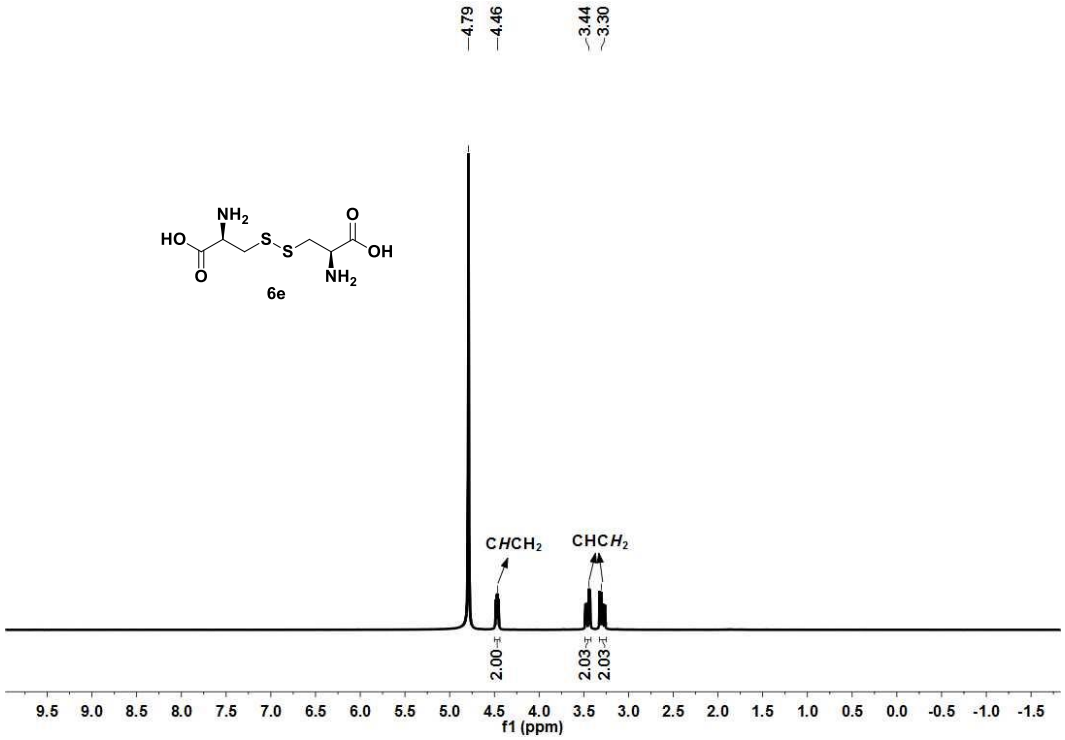

Figure S40. The ^{13}C NMR spectrum of **6e** in D_2O (4% NaOD)

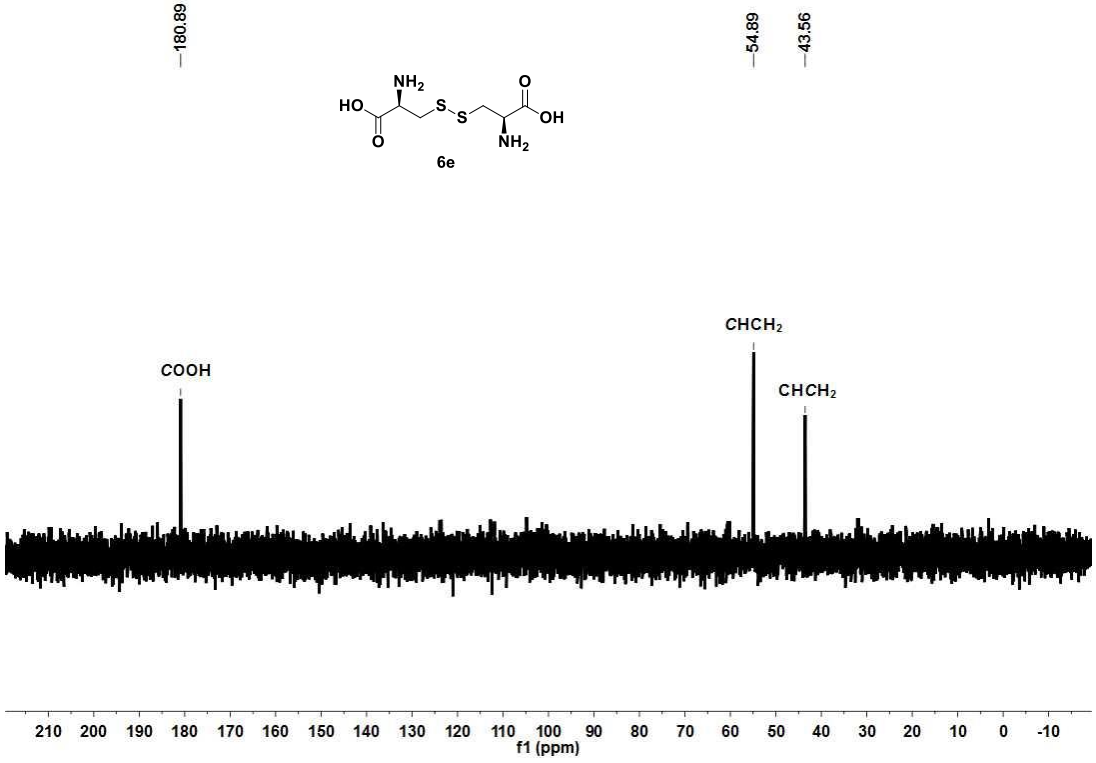

Figure S41. The ^{1}H NMR spectrum of **6f** in D_2O

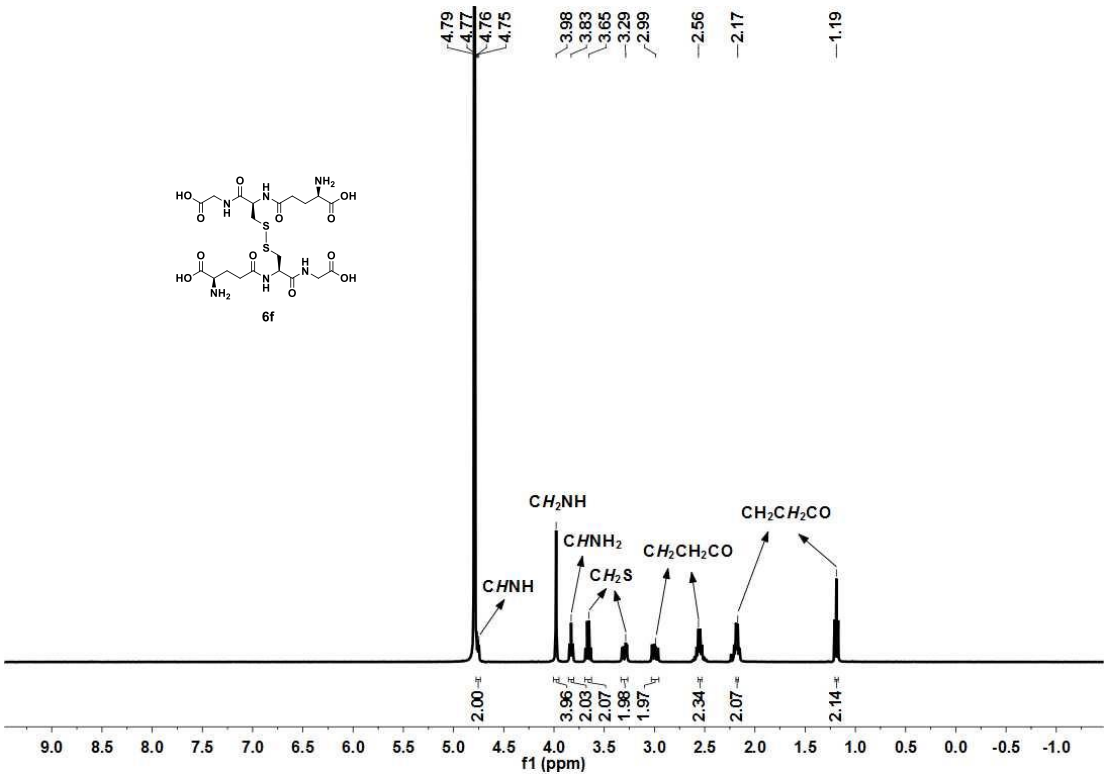

Figure S42. The ^{13}C NMR spectrum of **6f** in D_2O

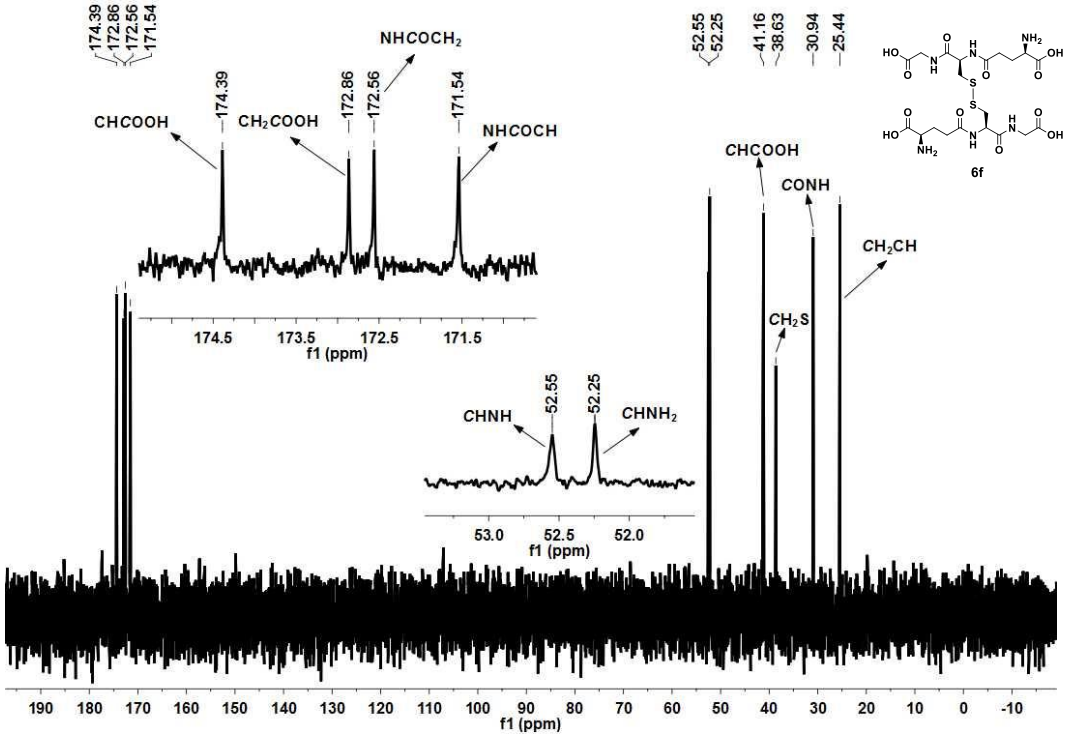

VIII. IR Spectra

Figure S43. The IR (film) spectrum of **2[PF$_6$]**

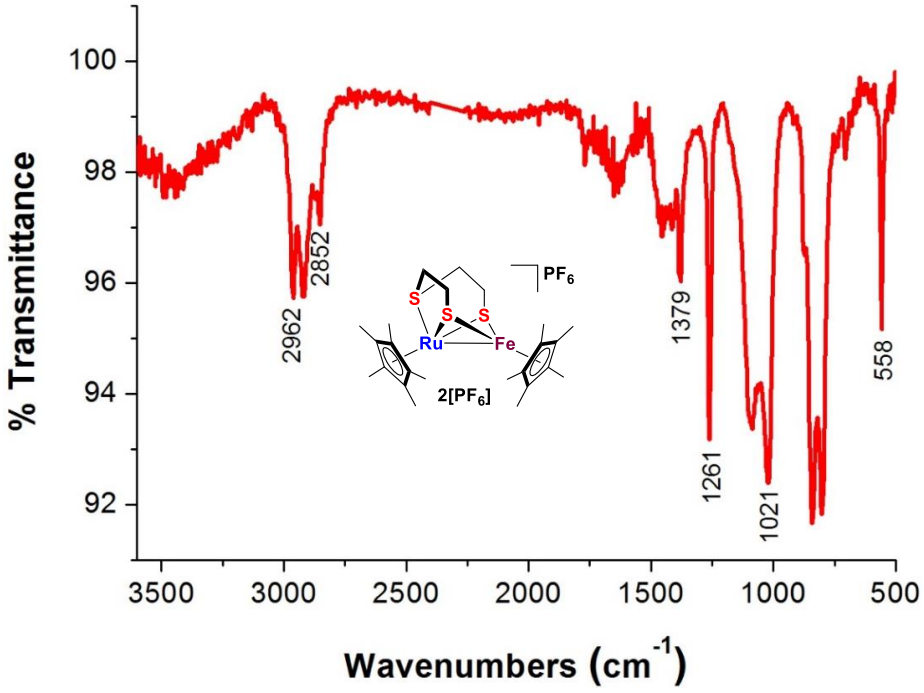

Figure S44. The IR (film) spectrum of **3**

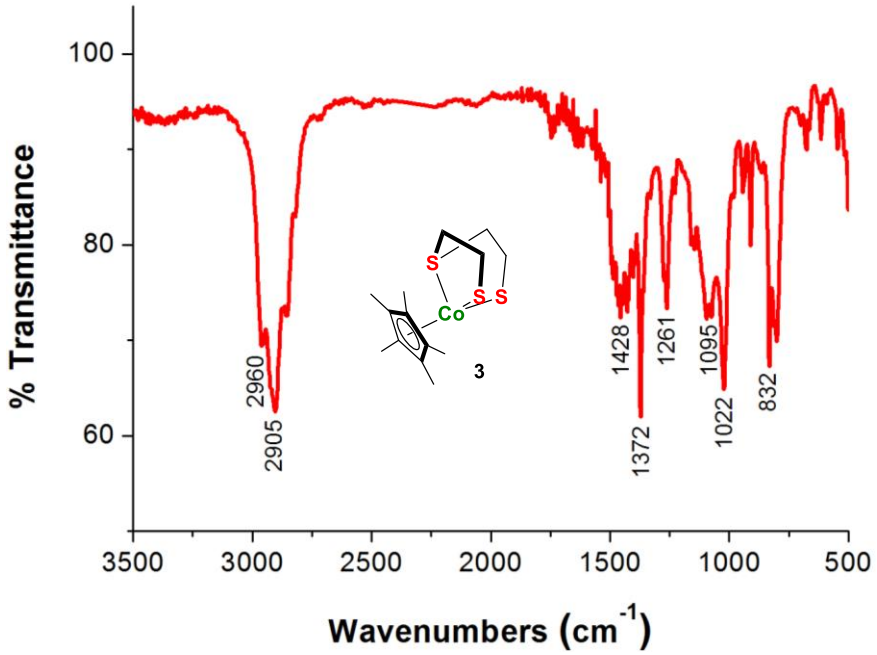

Figure S45. The IR (film) spectrum of **4a[BPh$_4$]**

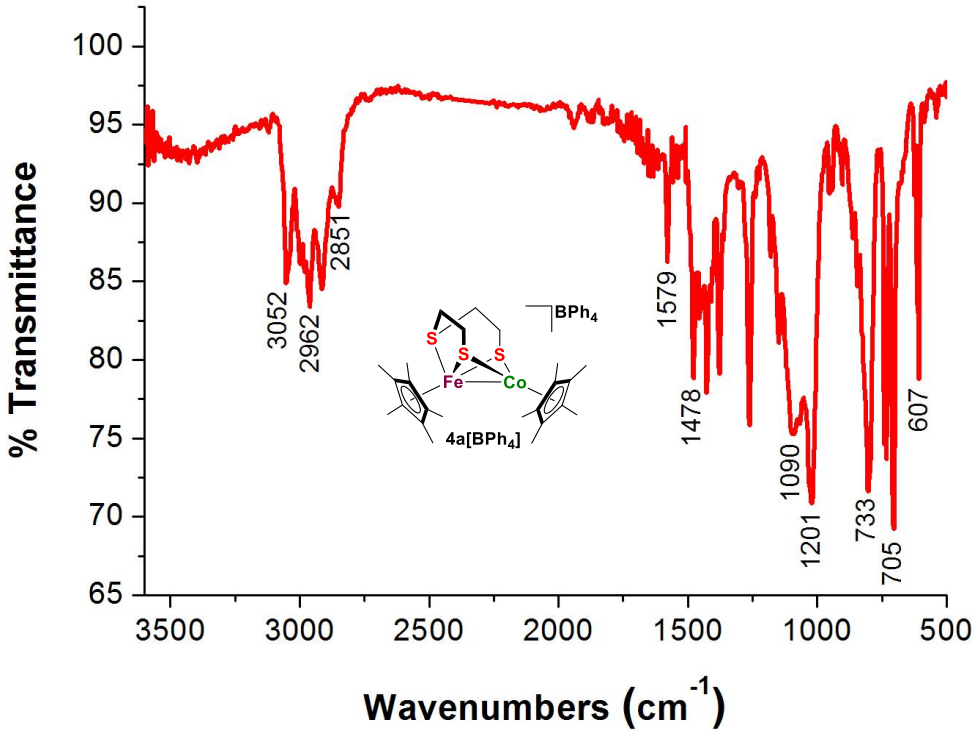

Figure S46. The IR (film) spectrum of **4b[BPh$_4$]**

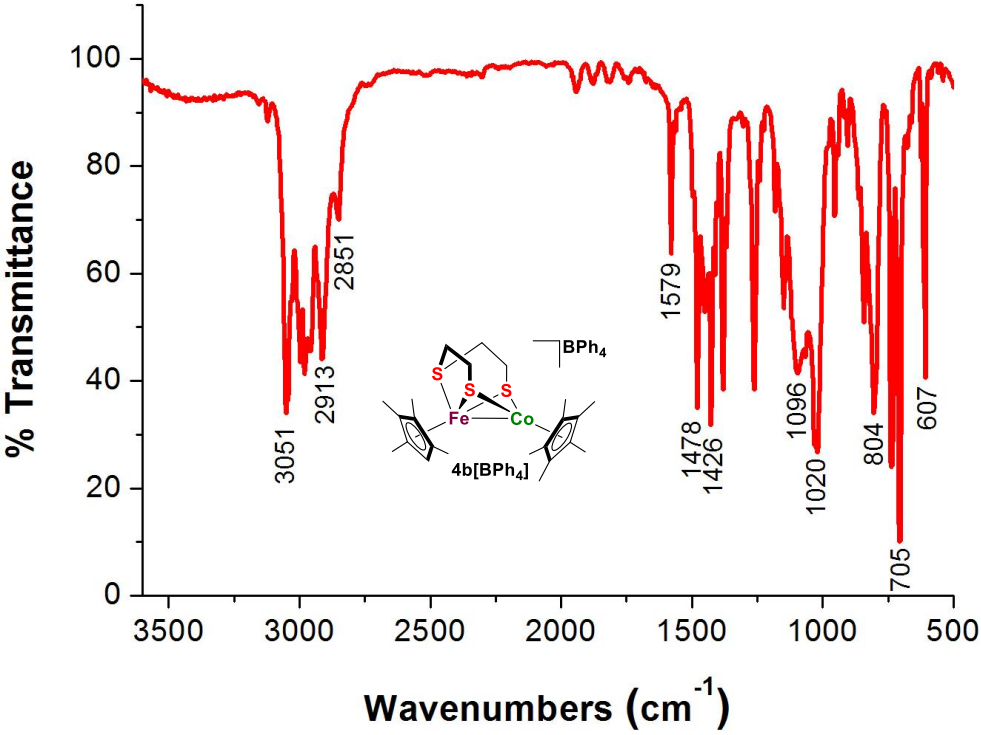

Figure S47. The IR (film) spectrum of **7[PF$_6$]$_2$**

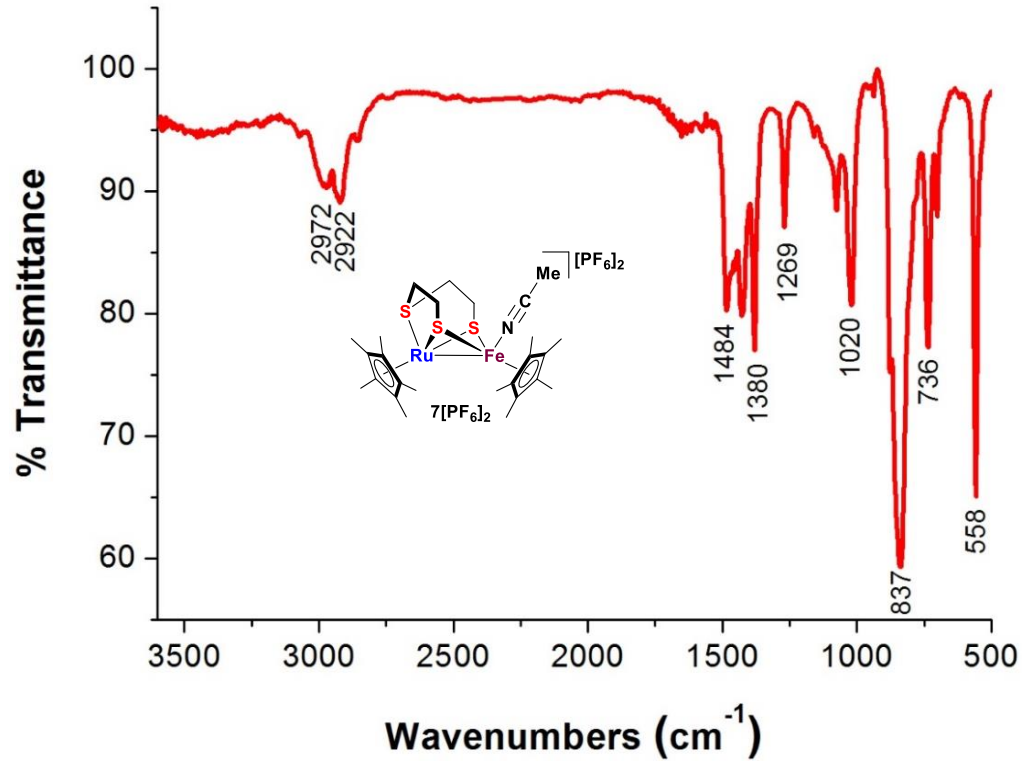

Figure S48. The IR (film) spectrum of **8[PF$_6$]**

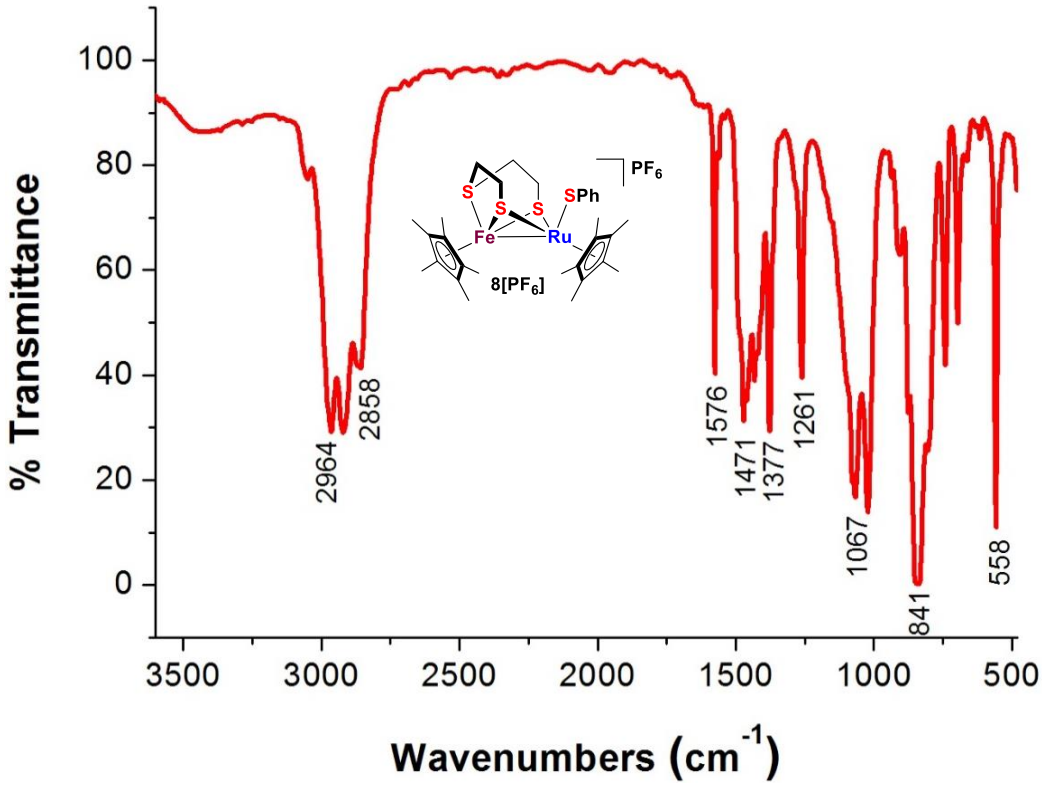

Figure S49. The IR (film) spectrum of **9[BPh$_4$]**